Article

Cell Reports

A Latent Propriospinal Network Can Restore Diaphragm Function after High Cervical Spinal Cord Injury

Graphical Abstract

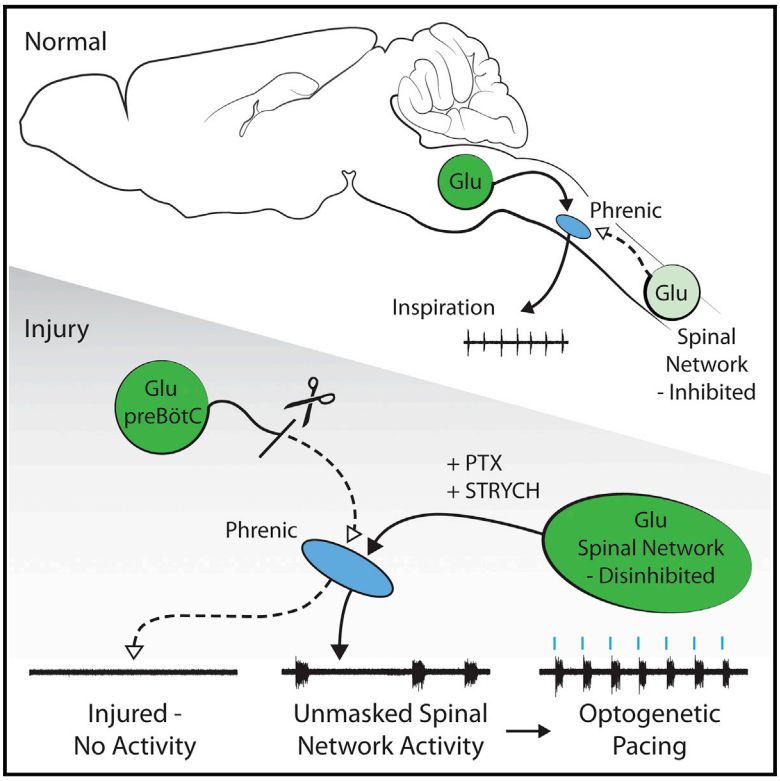

Highlights

- Blockade of inhibition uncovers a spinal cord network that elicits phrenic bursting
- Vglut2 interneurons were sufficient and necessary for induction of phrenic bursts
- Spinal-cord-derived phrenic bursting is dissociable from bona fide respiration
- This propriospinal network can be harnessed to allow diaphragm function after SCI

Authors

Jared M. Cregg, Kevin A. Chu, Lydia E. Hager, ..., Polyxeni Philippidou, Lynn T. Landmesser, Jerry Silver

Correspondence

jxs10@case.edu

In Brief

Cregg et al. uncover a spinal network that can direct diaphragm-innervating motoneurons to burst. This network is functionally independent of descending bulbospinal inspiratory circuits, which points to a different physiologic function. Targeting this network restores diaphragm function after cervical SCI.

Cregg et al., 2017, Cell Reports *21*, 654–665
October 17, 2017
https://doi.org/10.1016/j.celrep.2017.09.076

CellPress

OPEN ACCESS
CellPress

Cell Reports
Article

A Latent Propriospinal Network Can Restore Diaphragm Function after High Cervical Spinal Cord Injury

Jared M. Cregg,[1] Kevin A. Chu,[1] Lydia E. Hager,[2] Rachel S.J. Maggard,[2] Daimen R. Stoltz,[2] Michaela Edmond,[1] Warren J. Alilain,[2] Polyxeni Philippidou,[1] Lynn T. Landmesser,[1] and Jerry Silver[1,3,*]
[1]Department of Neurosciences, Case Western Reserve University, Cleveland, OH 44106, USA
[2]Spinal Cord and Brain Injury Research Center, Department of Neuroscience, University of Kentucky College of Medicine, Lexington, KY 40536, USA
[3]Lead Contact
*Correspondence: jxs10@case.edu
https://doi.org/10.1016/j.celrep.2017.09.076

SUMMARY

Spinal cord injury (SCI) above cervical level 4 disrupts descending axons from the medulla that innervate phrenic motor neurons, causing permanent paralysis of the diaphragm. Using an ex vivo preparation in neonatal mice, we have identified an excitatory spinal network that can direct phrenic motor bursting in the absence of medullary input. After complete cervical SCI, blockade of fast inhibitory synaptic transmission caused spontaneous, bilaterally coordinated phrenic bursting. Here, spinal cord glutamatergic neurons were both sufficient and necessary for the induction of phrenic bursts. Direct stimulation of phrenic motor neurons was insufficient to evoke burst activity. Transection and pharmacological manipulations showed that this spinal network acts independently of medullary circuits that normally generate inspiration, suggesting a distinct non-respiratory function. We further show that this "latent" network can be harnessed to restore diaphragm function after high cervical SCI in adult mice and rats.

INTRODUCTION

Inspiration—the act of drawing air into the lungs—is executed primarily by the diaphragm, which contracts ~20,000 times per day and 10^8 times over the average human lifespan. The diaphragm is solely innervated by phrenic motor neurons (PMNs), which are anatomically positioned at spinal cord levels C3-5/6. Thus, injury to the cervical spinal cord severely compromises diaphragm function.

Excitatory circuits of the pre-Bötzinger complex (preBötC), located in the ventrolateral medulla, generate inspiration and relay inspiratory drive to PMNs via a medullary premotor nucleus termed the rostral ventral respiratory group (rVRG; Smith et al., 1991). Neurons of the rVRG maintain bulbospinal projections that synapse directly with PMNs (Davies et al., 1985; Dobbins and Feldman, 1994; Duffin and van Alphen, 1995; Ellenberger and Feldman, 1988; Ellenberger et al., 1990); therefore, it is well established that rhythmic PMN bursts arise from circuits rostral to the spinomedullary junction. Evidence that rVRG axons make direct synaptic contact with PMNs comes from studies examining cross-correlation between rVRG units and phrenic nerve activity, which exhibit 1- to 2-ms latencies typical of monosynaptic connections (Davies et al., 1985; Duffin and van Alphen, 1995). Additional evidence comes from anatomical studies demonstrating close apposition of rVRG axons, identified by anterograde labeling, with the dendritic arbors of retrogradely labeled PMNs (Ellenberger and Feldman, 1988; Lane et al., 2008). Also, synapses between rVRG axon terminals and PMNs have been identified at the ultrastructural level (Ellenberger et al., 1990).

The simplest model, which is widely accepted, is that PMN bursts are always directly evoked by rVRG input. Nonetheless, there are also data indicating that, in the absence of supraspinal (rVRG) input, PMN activity can be initiated centrally by various pharmacological manipulations (Coglianese et al., 1977; Ghali and Marchenko, 2016; Reinoso et al., 1996; Viala et al., 1979; Zimmer and Goshgarian, 2007) or by electrical stimulation (Huang et al., 2016; Kowalski et al., 2013). Although it has been suggested that this activity might be generated by a spinal analog of the preBötC (Ghali and Marchenko, 2016), the origin of this activity has always been elusive. Indeed, it is largely unclear whether this PMN activity is caused by pharmacologic/electrical action on PMNs themselves or whether these manipulations engage propriospinal neurons, which are also known to synapse with PMNs (Dobbins and Feldman, 1994; Lane et al., 2008; Lipski et al., 1993; Lois et al., 2009). Importantly, there is no existing evidence that, when isolated from the medulla, propriospinal neurons can generate spontaneous PMN burst activity.

If there is a population of propriospinal neurons that can generate PMN bursts, then it is important to determine whether these interneurons simply relay inspiratory drive from the preBötC (e.g., preBötC → rVRG → interneuronal burst population → PMNs) or whether these neurons act as part of some other independent system—and what relevance this system might have. In this study, we establish an ex vivo model of spinal cord injury (SCI) and combine this model with pharmacologic and optogenetic perturbations to investigate whether propriospinal circuits are capable of evoking PMN bursts. We identify a recurrent

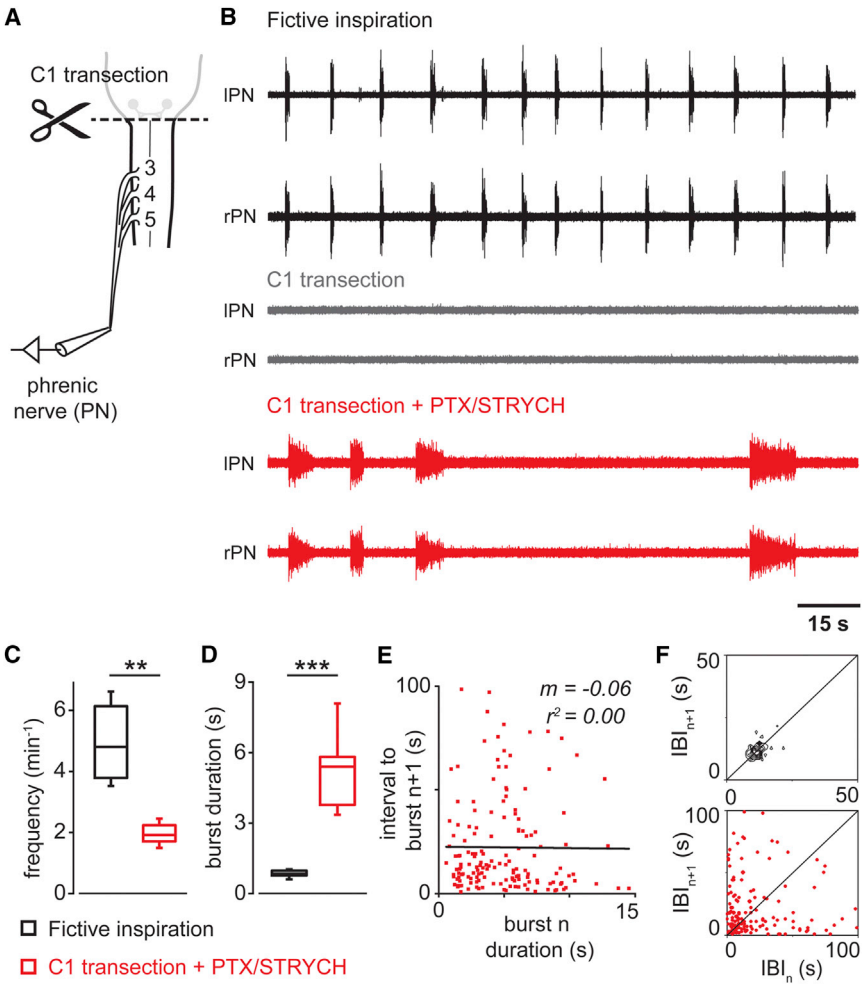

Figure 1. After C1 Transection, Blockade of Inhibitory Synaptic Transmission Initiates Persistent PMN Bursting

(A) Ex vivo preparation (P2–P4) consists of medulla and cervical through sacral spinal cord. Suction recording electrodes were placed on the phrenic nerves as they enter the pleural cavity.

(B) Spinal cord medullary preparations exhibit fictive inspiration. Phrenic nerve inspiratory activity is abolished after a C1 transection injury. Blockade of fast inhibition (+PTX/STRYCH) initiates spontaneous PMN bursting in the absence of descending bulbospinal input.

(C) Spontaneous spinal-cord-derived PMN bursting initiated by blockade of fast inhibition exhibits a slower frequency as compared with fictive inspiration (n = 8 mice; **p = 0.0019, U = 62, Mann-Whitney U test).

(D) PMN bursting initiated by blockade of fast inhibition exhibits a significantly longer burst duration as compared with fictive inspiration (n = 8 mice; ***p = 0.00009, F(1, 7.1) = 62.1, Welch's ANOVA).

(E) Burst duration for individual PMN bursts (n) initiated by blockade of fast inhibition does not predict timing or onset of subsequent bursts (n + 1, m = −0.06, r^2 = 0.00).

(F) Poincaré analysis of variability in interburst interval (IBI). Fictive inspiration is highly rhythmic (contour plot falls on line of identity for IBI_n versus IBI_{n+1}). Spinal-cord-derived PMN bursting does not exhibit a stable rhythm (contours do not fall on line of identity).

See also Figures S1 and S2.

excitatory network that is both sufficient and necessary for PMN bursting in the absence of the medulla and show that activity generated by this network is dissociable from bona fide inspiration. Furthermore, we demonstrate that this network can be used to promote diaphragm function after SCI in adult mice and rats.

RESULTS

Blockade of Inhibitory Synaptic Transmission Initiates Persistent PMN Bursting

We first established an ex vivo model of cervical SCI for tractable interrogation of phrenic premotor network organization. Mouse ex vivo preparations exhibit fictive inspiration (Figures 1A, 1B, and S1A). Inspiratory frequency in ex vivo preparations is depressed relative to in vivo conditions, due to lack of vagal feedback, as well as the relatively cooler temperatures required for maintaining the preparation during recording (23°C–26°C). In these neonatal preparations (post-natal day [P]2–P4), we found that a C1 lateral hemisection eliminates phrenic nerve inspiratory burst activity on the side ipsilateral to the lesion (Figure S1B, n = 8) and that complete transection at C1 arrests fictive inspiratory activity in both phrenic nerves (Figures 1B and S1C, n = 8). Since these data phenocopy well-characterized physiology of the adult mammal after SCI (Alilain et al., 2008), we proceeded to use this ex vivo preparation to understand the functional organization of phrenic premotor circuits.

We next examined whether spinal premotor circuits are capable of generating PMN bursts given tonic excitatory input. After a C1 transection injury, we found that bath application of NMDA/5HT elicited very modest PMN unit activity in 50% of cases (Figure S2A, n = 2 of 4). This unit activity did not exhibit any noticeable patterning between the left and right phrenic nerves, and PMNs did not exhibit any clear bursts. In contrast, application of NMDA/5HT evoked robust locomotor-like bursting from the ventral roots of the L2 segment, which exhibited right/left alternation (Figure S2B).

To further address whether an excitatory stimulus could evoke PMN bursts in the absence of medullary input, we used an optogenetic strategy to stimulate cervical Vglut2+ neurons. We found that, after complete C1 transection, 30 s of continuous photostimulation of the ventral cervical spinal cord of *Vglut2^{Cre};R26R^{ChR2}* preparations generated only modest PMN unit activity at light onset, with unit firing tapering off over the course of the photostimulation paradigm (Figure S2C). We examined PMN responses at multiple light intensities (10%–100%), different light stimulus frequencies (20 Hz, 50 Hz), and different pulse durations

(20 ms, 100 ms) and found that continuous light generated the strongest response, consisting solely of PMN unit activity but no PMN bursts (Figure S2C). In contrast, photostimulation of the lumbar cord evoked fictive locomotion (Hägglund et al., 2010), with alternating burst activity between right and left L2 ventral roots (Figure S2D). Together, these results indicate that simply increasing excitation in the absence of medullary input does not evoke PMN burst activity.

These data suggest either that the contribution of interneurons to PMN output is diminutive or that inhibition suppresses the action of excitatory interneurons under these conditions. To test these alternatives, we examined PMN output after blockade of fast inhibitory synaptic transmission. Unexpectedly, bath application of picrotoxin (PTX) and strychnine (STRYCH) in the absence of the medulla initiated spontaneous, bilaterally coordinated PMN bursting (Figure 1B). The frequency of spontaneous PMN bursting caused by blocking inhibition was much slower than that of fictive inspiration (Figure 1C). Spinal-cord-derived PMN bursts also exhibited a significantly longer burst duration compared with fictive inspiratory bursts (Figure 1D). The duration of each individual spontaneous PMN burst did not predict the onset of subsequent bursts (Figure 1E). Finally, whereas fictive inspiration was highly rhythmic (Figure 1F, top), spontaneous PMN bursting observed in the absence of inhibition was not rhythmic (Figure 1F, bottom).

Excitatory Interneurons Are Sufficient and Necessary for Spinal-Cord-Derived PMN Bursting

Spinal-cord-derived PMN bursting initiated by blockade of inhibitory synaptic transmission may be caused by two distinct mechanisms: First, bursts could arise from PMNs themselves via synchronization of subthreshold activity in electrically coupled dendritic arbors (Tresch and Kiehn, 2000). Previous electrophysiological analyses, however, have suggested that PMNs do not exhibit electrical coupling via gap junctions (Lipski, 1984). Second, PMN bursts could arise from recurrent excitatory premotor networks. To distinguish between these possibilities, we examined PMN burst generation after washing out Ca^{2+}, which is required for synaptic transmission. Ca^{2+} washout completely eliminated spinal-cord-derived PMN bursts (Figure S3A). Moreover, we found that blockade of NMDA and non-NMDA glutamate receptors also abolished spontaneous PMN bursting (Figure S3B). These data indicate that excitatory presynaptic input is required for spontaneous PMN bursting after blockade of inhibitory synaptic transmission.

We next tested whether PMN bursts could be evoked by stimulation of cervical glutamatergic interneurons. In PTX/STRYCH disinhibited preparations from $Vglut2^{Cre};R26R^{ChR2}$ mice, a series of 200-ms photostimuli centered on the ventral cervical spinal cord was sufficient to evoke bilaterally coordinated PMN bursting (Figures 2A–2D). PMN bursting could be driven at a frequency similar to that of fictive inspiration (Figures 2D–2F, ~5 bursts per min^{-1}). The duration of individual burst episodes was significantly shorter during trains of photostimulation compared with those observed spontaneously (Figure 2G). Light-evoked PMN bursts do not simply reflect direct activation of PMNs by Vglut2+ sensory or bulbospinal fibers, because stimulation of Vglut2+ fibers in the absence of PTX/STRYCH did not evoke PMN bursts (Figure S2C). Additionally, the brief 200-ms photostimulus caused activity that lasted on the order of seconds (Figures 2C, 2D, 2G, and 2H). This suggests that the stimulus is recruiting recurrent excitatory premotor networks.

Blockade of NMDA and non-NMDA glutamate receptors abolished light-evoked PMN burst activity (Figure 2H), indicating a presynaptic origin of light-evoked bursts. Although it is well known that lumbar motor neurons release glutamate and express Vglut2 (Mentis et al., 2005; Nishimaru et al., 2005; Talpalar et al., 2011), we observed only sparse $Vglut2^{Cre}$-mediated recombination of an EYFP-reporter allele in putative PMNs (Figure 2B, arrow). To directly examine $Vglut2^{Cre}$-mediated recombination in PMNs, we retrogradely traced PMNs by intrapleural injection of CTB-555 (Figures S4A–S4C). PMNs labeled by CTB-555 were positioned between the medial and lateral motor columns in spinal cord levels C3–C5 (Figures 3A and 3B). 27.2% of CTB-labeled PMNs expressed LacZ in $Vglut2^{Cre};Tau^{lsl\text{-}LacZ}$ mice (50/184 neurons; n = 4; Figures S4A–S4C).

We next performed in situ analysis to assess whether PMNs express *Vglut2* mRNA (Figures S4D–S4F). While some motor neurons of the lateral column expressed *Vglut2*, most PMNs lacked expression (n = 4; 4/104 neurons; Figures S4D–S4F). These data indicate that $Vglut2^{Cre}$-mediated recombination in a subset of PMNs is caused by transient, rather than sustained, *Vglut2* expression.

After Ca^{2+} washout, stimulation of ChR2-expressing PMNs in $Vglut2^{Cre};R26R^{ChR2}$ mice evoked only minor PMN unit activity but no PMN bursts (Figures S4I and S4J). These results indicate that light-evoked bursts arise from excitatory premotor networks rather than from direct stimulation of PMNs.

Direct Stimulation of PMNs Is Not Sufficient to Evoke PMN Bursts

To further test whether stimulation of PMNs would be sufficient to evoke PMN bursts, we used a $ChAT^{Cre}$ allele to allow motor-neuron-specific expression of ChR2 (Figure 3B). 99.1% of PMNs expressed ChR2-EYFP in $ChAT^{Cre};R26R^{ChR2}$ mice (216/218 neurons; n = 7; Figures S4G and S4H). We also observed ChR2-EYFP expression in cholinergic interneurons (Figure 3B, arrows), which represent a small fraction of cervical spinal interneurons (Barber et al., 1984).

After C1 transection and blockade of inhibitory synaptic transmission, 200-ms $ChAT^{Cre};R26R^{ChR2}$ photostimulation resulted in PMN unit activity for 193 ms ± 6 ms, but it did not evoke bursts that outlasted the stimulus duration (Figure 3C). In comparison, 200-ms photostimulation of Vglut2+ interneurons resulted in a burst of PMN activity that lasted for 3,635 ms ± 556 ms (Figures 3C and 3D). We examined whether varying the stimulus duration in $ChAT^{Cre};R26R^{ChR2}$ preparations would lead to burst responses lasting longer than the light stimulus. Photostimuli of 200–4,000 ms evoked PMN unit activity that lasted only for the duration of the photostimulus (Figures 3E and 3F). Since light-evoked PMN unit activity persisted after Ca^{2+} washout, it is caused by direct stimulation of PMNs rather than ChR2+ cholinergic interneurons (Figures 3E and 3F). Lastly, after Ca^{2+} washout, photostimulation of PMNs in $ChAT^{Cre};R26R^{ChR2}$ mice caused a much more robust unit response than photostimulation of PMNs in $Vglut2^{Cre};R26R^{ChR2}$ mice (Figures S4I and S4J). This

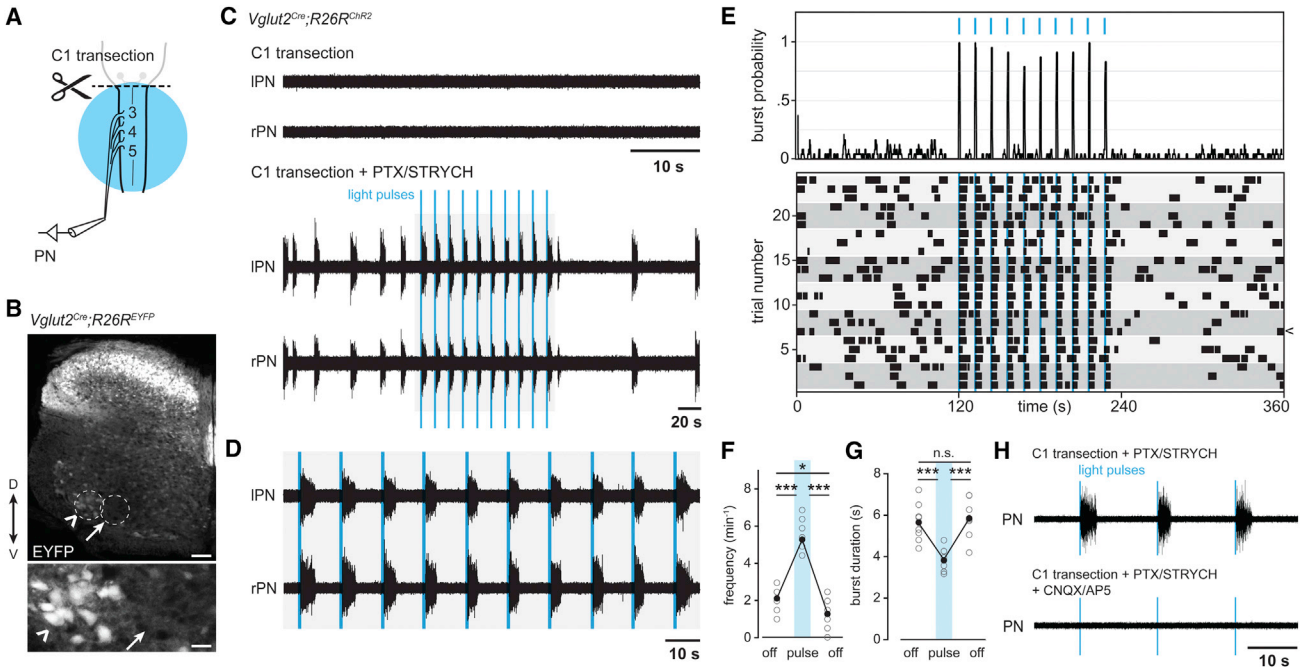

Figure 2. Excitatory Neurons Are Sufficient and Necessary for PMN Burst Activity in the Absence of Bulbospinal Input

(A) Experimental ex vivo paradigm for photostimulation of cervical Vglut2+ neurons.

(B) Distribution of neurons exhibiting *Vglut2*^{Cre}-induced expression of EYFP from a *R26R*^{EYFP} reporter allele in cervical spinal cord level C5. Vglut2+ neurons are situated in spinal cord laminae I–X. Motor neurons identified by their position in lamina IX also exhibit Cre-induced expression of EYFP (arrowheads); however, a region corresponding to the location of the phrenic motor nucleus lacked EYFP+ soma (arrows). Scale bar: top, 100 μm; bottom, 30 μm. D, dorsal; V, ventral.

(C) After complete C1 transection, spinal cord preparations exhibit no PMN activity. PTX/STRYCH application induces bilaterally coordinated bursting of PMNs, and single bursts can be evoked by ChR2-mediated stimulation of Vglut2+ glutamatergic neurons with 200-ms pulses of blue light. Light was pulsed at a frequency of 5 min^{-1}.

(D) Inset from (C).

(E) Burst probability plot and raster plot for PTX/STRYCH-induced bursts. Individual trials are aligned by light onset, and gray boxes are used to highlight independent biological replicates (3 trials per animal; n = 8 mice).

(F) Burst frequency is increased during photostimulation (n = 8 mice; ***p = 8.5 × 10^{-11} before versus during photostimulation; ***p = 6.2 × 10^{-11} during versus after photostimulation; *p = 0.013 before versus after photostimulation; F(2, 21) = 156.5, one-way ANOVA and post hoc Tukey-Kramer honest significant difference [HSD]). n.s., not significant.

(G) Burst duration is significantly reduced during photostimulation (n = 8 mice, ***p = 0.0007 before versus during photostimulation; ***p = 0.0002 during versus after photostimulation; F(2, 21) = 14.6, one-way ANOVA and post hoc Tukey-Kramer HSD).

(H) PMN bursting evoked by stimulation of Vglut2+ neurons requires glutamate transmission (n = 2 mice).

See also Figures S3 and S4.

is consistent with our anatomical data demonstrating that only a subset of PMNs exhibit *Vglut2*^{Cre}-mediated recombination (Figure S4C). Together, these data indicate that direct stimulation of PMNs is not sufficient to evoke sustained PMN bursts. We conclude that PMN bursts arise from recurrent excitatory premotor networks.

Dissociation of Spinal-Cord-Derived PMN Bursting from Bona Fide Inspiration

Our results provide evidence for an excitatory spinal cord network that can evoke PMN bursting. To address whether this network relays excitatory inspiratory drive from higher order medullary nuclei (e.g., preBötC → rVRG → interneuronal burst population → PMNs), we examined PMN activity after blockade of inhibition in spinomedullary preparations. Interestingly, we observed two distinct modes of PMN bursting under these conditions: high frequency/short duration and low frequency/long duration (Figures 4A and 4B, +PTX/STRYCH). We reasoned that these distinct modes of PMN bursting reflect the action of two distinct premotor networks: PMN bursts of shorter duration are likely driven by the preBötC because they exhibit a frequency and duration similar to those of fictive inspiration (Figure 4B), and the longer PMN bursts are likely driven by excitatory spinal cord network activity, which emerges following blockade of inhibition.

To test this, we performed a lateral C1 hemisection lesion to eliminate descending medullary input to PMNs on the right side. We found that C1 hemisection eliminated short-duration bursts only on the side ipsilateral to the lesion (Figure 4A, diamonds). Notably, synchronous long-duration PMN bursts were retained on both sides (Figures 4A and 4B). We conclude that the high-frequency/short-duration bursts are of medullary origin, and long-duration bursts are of spinal cord origin. Importantly, these experiments demonstrate that, in disinhibited

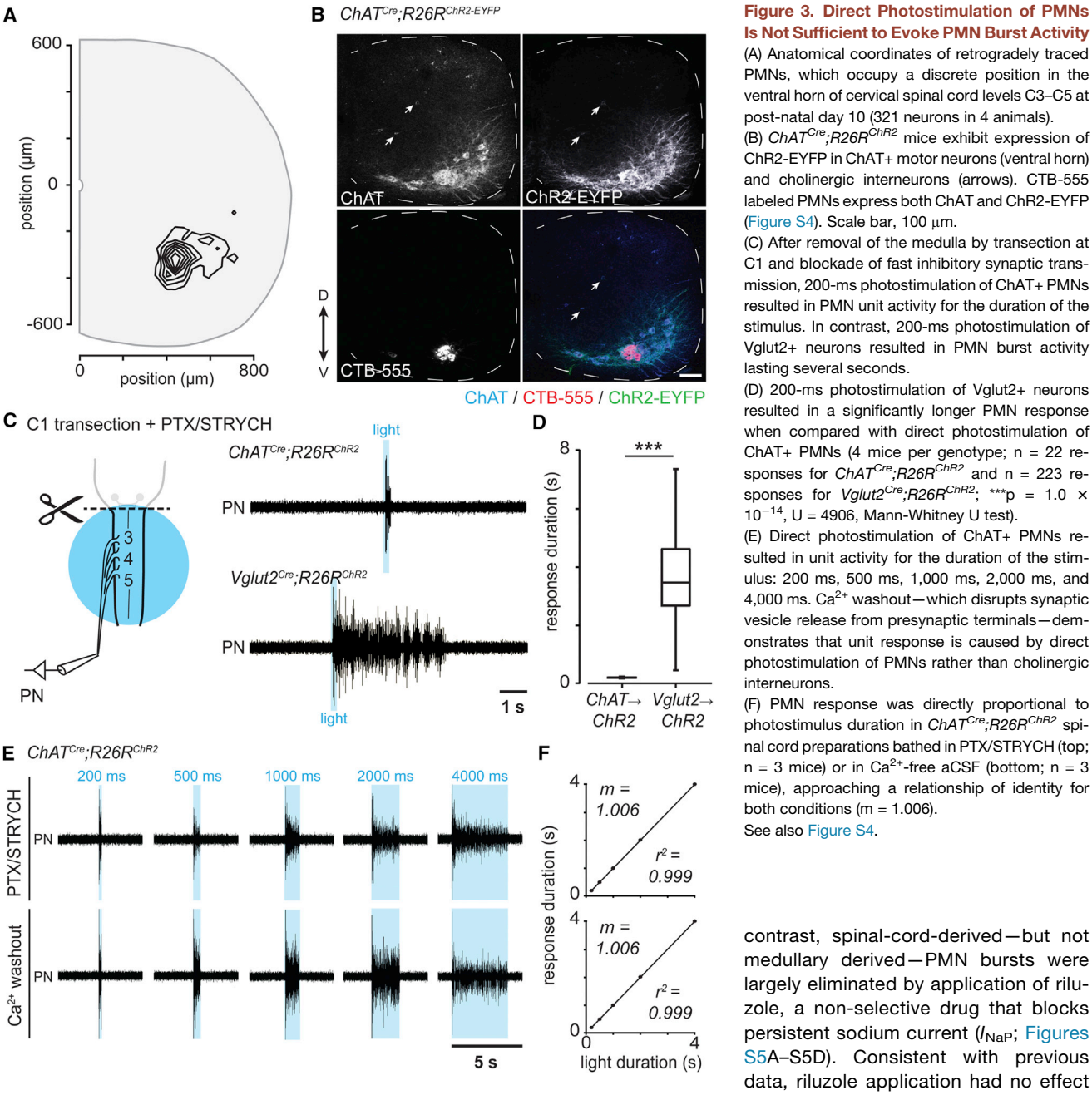

Figure 3. Direct Photostimulation of PMNs Is Not Sufficient to Evoke PMN Burst Activity

(A) Anatomical coordinates of retrogradely traced PMNs, which occupy a discrete position in the ventral horn of cervical spinal cord levels C3–C5 at post-natal day 10 (321 neurons in 4 animals).

(B) *ChAT*^{Cre};*R26R*^{ChR2} mice exhibit expression of ChR2-EYFP in ChAT+ motor neurons (ventral horn) and cholinergic interneurons (arrows). CTB-555 labeled PMNs express both ChAT and ChR2-EYFP (Figure S4). Scale bar, 100 μm.

(C) After removal of the medulla by transection at C1 and blockade of fast inhibitory synaptic transmission, 200-ms photostimulation of ChAT+ PMNs resulted in PMN unit activity for the duration of the stimulus. In contrast, 200-ms photostimulation of Vglut2+ neurons resulted in PMN burst activity lasting several seconds.

(D) 200-ms photostimulation of Vglut2+ neurons resulted in a significantly longer PMN response when compared with direct photostimulation of ChAT+ PMNs (4 mice per genotype; n = 22 responses for *ChAT*^{Cre};*R26R*^{ChR2} and n = 223 responses for *Vglut2*^{Cre};*R26R*^{ChR2}; ***p = 1.0 × 10^{-14}, U = 4906, Mann-Whitney U test).

(E) Direct photostimulation of ChAT+ PMNs resulted in unit activity for the duration of the stimulus: 200 ms, 500 ms, 1,000 ms, 2,000 ms, and 4,000 ms. Ca^{2+} washout—which disrupts synaptic vesicle release from presynaptic terminals—demonstrates that unit response is caused by direct photostimulation of PMNs rather than cholinergic interneurons.

(F) PMN response was directly proportional to photostimulus duration in *ChAT*^{Cre};*R26R*^{ChR2} spinal cord preparations bathed in PTX/STRYCH (top; n = 3 mice) or in Ca^{2+}-free aCSF (bottom; n = 3 mice), approaching a relationship of identity for both conditions (m = 1.006).

See also Figure S4.

preparations, excitatory medullary and spinal cord premotor networks do not interact; one type of bursting does not drive the other.

We next examined whether medullary and spinal cord premotor networks exhibit differential pharmacological sensitivity. Opioids are known to depress inspiration via direct action on preBötC circuits (Gray et al., 1999). In spinomedullary preparations, bursts of medullary origin exhibited slower frequency, smaller amplitude, and shorter duration in response to bath application of the μ-opioid agonist DAMGO (Figures 4A and 4C), whereas bursts of spinal cord origin were remarkably insensitive to DAMGO (Figures 4A and 4C). In contrast, spinal-cord-derived—but not medullary derived—PMN bursts were largely eliminated by application of riluzole, a non-selective drug that blocks persistent sodium current (I_{NaP}; Figures S5A–S5D). Consistent with previous data, riluzole application had no effect on medullary derived inspiratory burst frequency (Figures S5A and S5B; Thoby-Brisson et al., 2009) but shortened both the amplitude and duration of inspiratory bursts (Figures S5C and S5D; Peña et al., 2004). Together, these pharmacological manipulations demonstrate that spinal-cord-derived PMN bursting is dissociable from bona fide inspiration.

Spontaneous Spinal-Cord-Derived PMN Bursts Originate in the Thoraco-lumbar Cord

To further examine the anatomical origin of spontaneous burst initiation after blockade of inhibitory synaptic transmission, we simultaneously recorded from the phrenic nerve and the L2

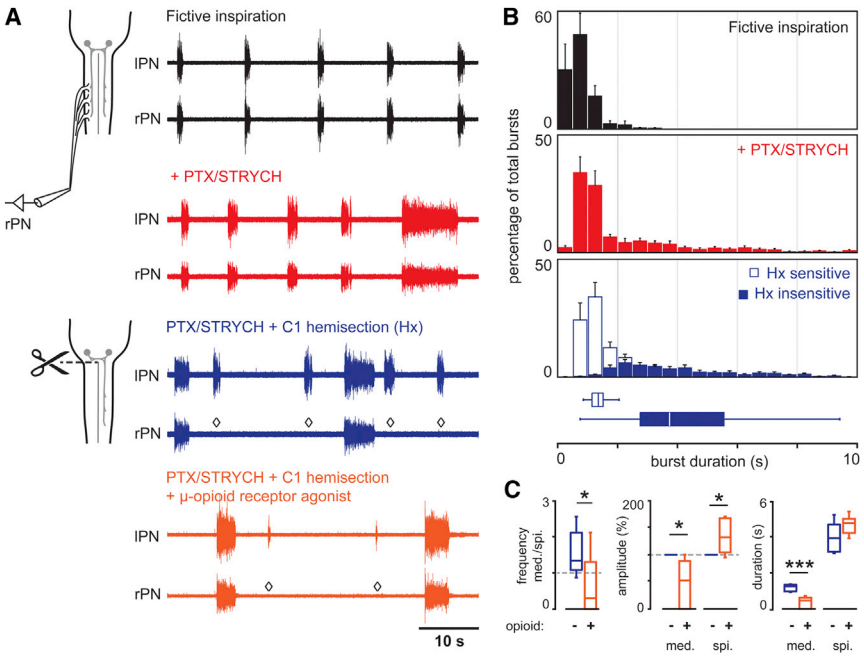

Figure 4. Spinal-Cord-Derived PMN Bursting Is Independent of Bona Fide Inspiration

(A) In spinomedullary preparations, blockade of fast inhibitory synaptic transmission evoked two distinct modes of PMN bursting—high frequency/short duration and low frequency/long duration (red traces). C1 hemisection (right side, rPN) eliminated high-frequency/short-duration bursts, whereas low-frequency/long-duration bursts were retained on both the lesioned and intact sides (blue; n = 8). Application of the μ-opioid receptor agonist DAMGO selectively depressed the amplitude and duration of medullary derived—but not spinal-cord-derived—PMN bursts (orange). Open diamonds indicate absence of medullary derived PMN bursts on the side ipsilateral to C1 hemisection.

(B) Dual modes of PMN bursting visualized in burst duration histograms (n = 8). Fictive inspiratory bursts (black) are concentrated in the range of 0–2.5 s. PTX/STRYCH application (red) causes a shift in the distribution: while a majority of bursts are 0–2.5 s in duration, a second population of bursts of longer duration emerges, with significantly longer duration. C1 hemisection distinguishes medullary derived PMN bursts of high frequency/short duration (open bars) from spinal-cord-derived PMN bursts of low frequency/long duration (shaded bars), as shorter bursts are lost on the hemisected side. Data are mean ± SEM, n = 8.

(C) Left panel: application of the μ-opioid receptor agonist DAMGO caused medullary derived bursts to become less frequent than spinal-cord-derived bursts (n = 7 mice; *p = 0.038, t_{12} = 2.3, two-tailed t test). Middle panel: the opioid agonist selectively depressed the amplitude of medullary derived (med.)—but not spinal-cord-derived (spi.)—PMN bursts (n = 7 mice; *p = 0.0202 and U = 41 for med.; *p = 0.0204 and U = 41 for spi.; Mann-Whitney U test). Right panel: the opioid agonist selectively shortened medullary derived—but not spinal-cord-derived—PMN bursts (n = 7 mice; ***p = 3.6×10^{-5} for med. and t_{12} = 6.4, p = 0.0783 and t_{12} = 1.9 for spi., two-tailed t test).

See also Figure S5.

ventral root (Figure 5A). Previous work in the lumbar spinal cord has demonstrated that blockade of inhibitory synaptic transmission initiates synchronous bursting across multiple ventral roots (Bracci et al., 1996). This synchronous burst activity has been attributed to excitatory premotor circuits associated with locomotion (Bracci et al., 1996; Hägglund et al., 2010; Talpalar et al., 2011). Upon application of PTX/STRYCH in C1 transected preparations, we found that PMNs exhibited long-duration bursting synchronous with lumbar motor neurons in L2 (Figures 5A and 5B). Furthermore, PTX/STRYCH application caused similar bursting in the radial and musculocutaneous nerves (data not shown), suggesting that long-duration bursts generated by excitatory interneurons recruit motor neurons at every spinal level. Importantly, PMN bursting in the disinhibited cord was insensitive to application of the muscle acetylcholine receptor (AChR) antagonist d-tubocurarine (1.44 min^{-1} ± 0.35 min^{-1} before versus 1.29 min^{-1} ± 0.35 min^{-1} after; n = 2), demonstrating that spontaneous PMN bursts are recruited directly by an excitatory premotor network rather than indirectly via intercostal muscle sensory afferents (Decima et al., 1969).

To better define the location of networks generating spontaneous bursts in the disinhibited spinal cord, we transected the spinal cord at T8. Interestingly, regions of spinal cord rostral and caudal to the transection both continued to generate bursts, but these bursts were no longer synchronous, and the frequency of the bursts rostral to T8 was reduced (Figures 5A–5C). In a purely excitatory network, such as the early embryonic spinal cord or sinoatrial-atrioventricular (SA-AV) node coupling in the heart, burst initiation is determined by the most excitable population of cells. Our data suggest that the most excitable population of glutamatergic neurons in the disinhibited spinal cord resides caudal to T8 and that this population drives network-wide bursts. However, in their absence, other excitable populations of glutamatergic neurons rostral to T8 can take over and initiate network-wide bursts, albeit at a lower frequency (Figure 5C). We subsequently performed sequential rostral spinal cord transections and found that transection at C8 abolished spontaneous spinal-cord-derived PMN bursting (Figures 5A and 5C). Although C8 transection abolished *spontaneous* PMN bursting (Figures 5A and 5C), small PMN bursts could still be evoked by stimulation of cervical glutamatergic neurons in a subset of cases (n = 2 of 4 mice; Figures 5D and 5E). These data indicate that recurrent excitatory networks in the disinhibited spinal cord exhibit a gradient of excitability that is highest in the lumbar cord and lowest in the cervical cord (Figure 5F).

Spinal Cord Premotor Networks Can Restore Diaphragm Function after Hemiparalysis

A few previous studies have demonstrated that blockade of inhibitory synaptic transmission can initiate PMN activity in adult rodents (Ghali and Marchenko, 2016; Zimmer and Goshgarian, 2007). Although the nature of this activity was largely unclear, it was suggested that this activity might represent a spinal cord origin for respiratory rhythm (Ghali and Marchenko, 2016). Given

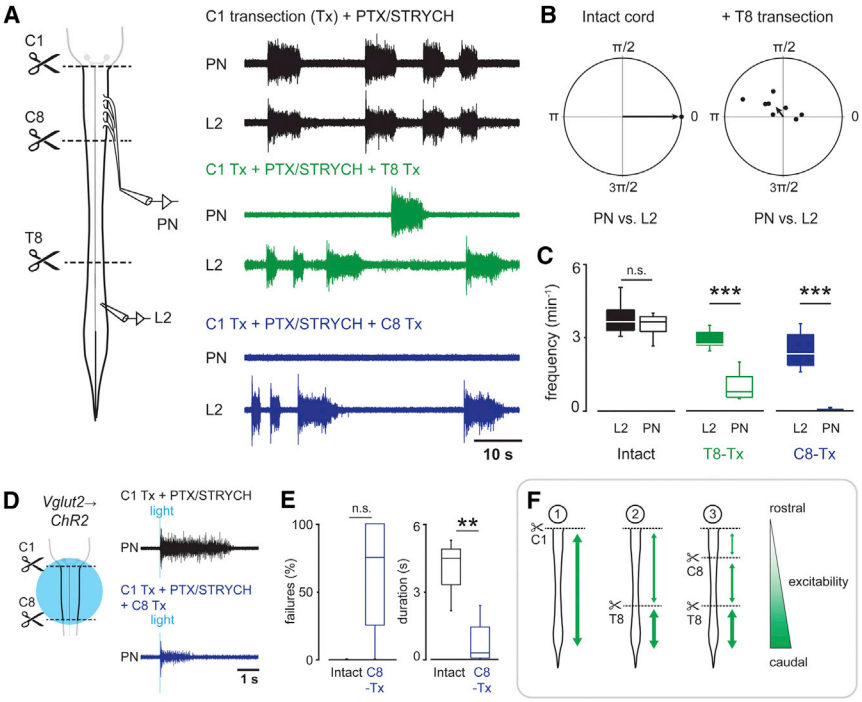

Figure 5. Spinal-Cord-Derived PMN Bursts Originate in the Thoraco-lumbar Cord

(A) In spinal cord preparations, blockade of fast inhibitory synaptic transmission initiated PMN bursting that was tightly coupled with L2 bursting. T8 transection disrupted PN/L2 coupling, and C8 transection eliminated PMN bursting initiated by blockade of inhibitory synaptic transmission.

(B) Phase diagrams demonstrate tight PN/L2 coupling after blockade of fast inhibitory synaptic transmission. Coupling was disrupted by T8 spinal cord transection.

(C) PN burst frequency versus L2 burst frequency. Sequential rostral spinal cord transections demonstrate that spontaneous PMN bursts originate in the thoraco-lumbar cord. PN burst frequency is significantly reduced relative to L2 after T8 transection (n = 8 mice; $p = 0.0704$ and $t_{14} = 0.4$ for intact cord, two-tailed t test; ***$p = 0.00093$ and $U = 64$ for T8-Tx, Mann-Whitney U test) and is virtually eliminated after C8 transection (n = 8 mice; ***$p = 0.00055$ and $U = 64$, Mann-Whitney U test). n.s., not significant.

(D) Although spontaneous PMN bursting is eliminated after C8 transection, small PMN bursts can still be evoked by ChR2 stimulation of Vglut2+ neurons in the cervical spinal cord.

(E) Bursts evoked by photostimulation of Vglut2+ neurons after C8 transection exhibited a higher failure rate (n = 4 mice; $p = 0.067$, $U = 12$, Mann-Whitney U test; n = 4 mice exhibited no failures when the spinal cord was intact, and n = 2 of 4 mice failed at a rate of 100% after C8 transection). *Vglut2*^{Cre}*;R26R*^{ChR2}-evoked response duration was much shorter after C8 transection compared with the intact spinal cord (n = 4 mice; **$p = 0.0092$, $F(1, 5.8) = 14.7$, Welch's ANOVA).

(F) Summary of findings. In the intact disinhibited spinal cord (1), low-frequency/long-duration bursts propagate within the rostrocaudal extent of the cord. After T8 transection (2), long-duration bursts propagate independently within the C1-T8 and T9-sacral segments. Long-duration bursts are generated at a higher frequency within the T9-sacral segment. After C8 transection, spontaneous, long-duration bursts are largely eliminated from the cervical cord but can still be evoked by photostimulation of Vglut2+ neurons. These findings indicate that spinal cord glutamatergic networks exhibit a gradient of excitability that is highest in the lumbar cord and lowest in the cervical cord. The rostrocaudal extent of burst propagation is indicated by green arrows, and the thickness of the green arrows represents excitability.

that hemisection lesions can dissociate spinal cord burst activity from bona fide inspiration (Figures 4A and 4B; also shown in Figure 6A for comparison with the adult), we examined whether similar lesions would dissociate PTX/STRYCH-initiated PMN activity from respiration in adult mice. In anesthetized mice >8 weeks old, C2 hemisection abolished diaphragm activity ipsilateral to the lesion (Figure 6B). Subsequent microinjection of PTX/STRYCH into the cervical spinal cord rapidly initiated activity in the paralyzed hemidiaphragm (Figure 6B, green arrows). This activity was largely independent of rhythmic inspiratory circuits of the preBötC, because medullary driven inspiratory bursts did not evoke weak unit or burst activity ipsilateral to the lesion (Figures 6B and 6C, indicated by diamonds). However, given the fast dynamics of mouse respiration (~90 min^{-1}), we found that long spinal-cord-derived bursts almost always overlapped with medullary derived respiratory bursts to some degree (Figures 6B and 6C).

To demonstrate that long-duration spinal-cord-derived bursts can occur independently of medullary derived bursts, we performed similar experiments in adult rats, which exhibited a slower respiratory rate than mice (~30 min^{-1}; Figure 6D). C2 hemisection lesions abolished diaphragm activity ipsilateral to the lesion (Figure 6D), and intrathecal application of PTX/STRYCH initiated spontaneous activity in the paralyzed hemidiaphragm (Figure 6D). Again, activity observed in the paralyzed hemidiaphragm (Figures 6D and 6E, green arrows) was independent of the preBötC, because medullary driven inspiratory bursts did not evoke weak unit or burst activity ipsilateral to the lesion (Figures 6D and 6E, diamonds). Likely owing to the slower dynamics of rat respiration, we observed several long spinal-cord-derived bursts that were clearly spaced between medullary derived inspiratory bursts (Figures 6D and 6E). In both adult mice and rats, we observed ipsilateral diaphragm activity after administration of PTX/STRYCH at the cervical level, suggesting that recurrent excitatory networks rostral to C8 (see evoked activity in Figures 5D and 5E) may give rise to spontaneous burst activity in vivo due to enhanced neural dynamics (37°C versus 23°C–26°C ex vivo). It is also likely that PTX/STRYCH diffused far beyond the initial site of application, because we noted spastic-like movements of the hindlimbs. These data are largely consistent with our ex vivo data (Figure 6A), indicating that the spinal network we characterize in neonatal preparations has a correlate in adult animals. Together, these data demonstrate that spontaneous spinal-cord-derived PMN bursting is generated independently of respiratory rhythm in adult animals (Figure 7) and may be harnessed to promote diaphragm activity in the absence of descending bulbospinal input in the context of SCI.

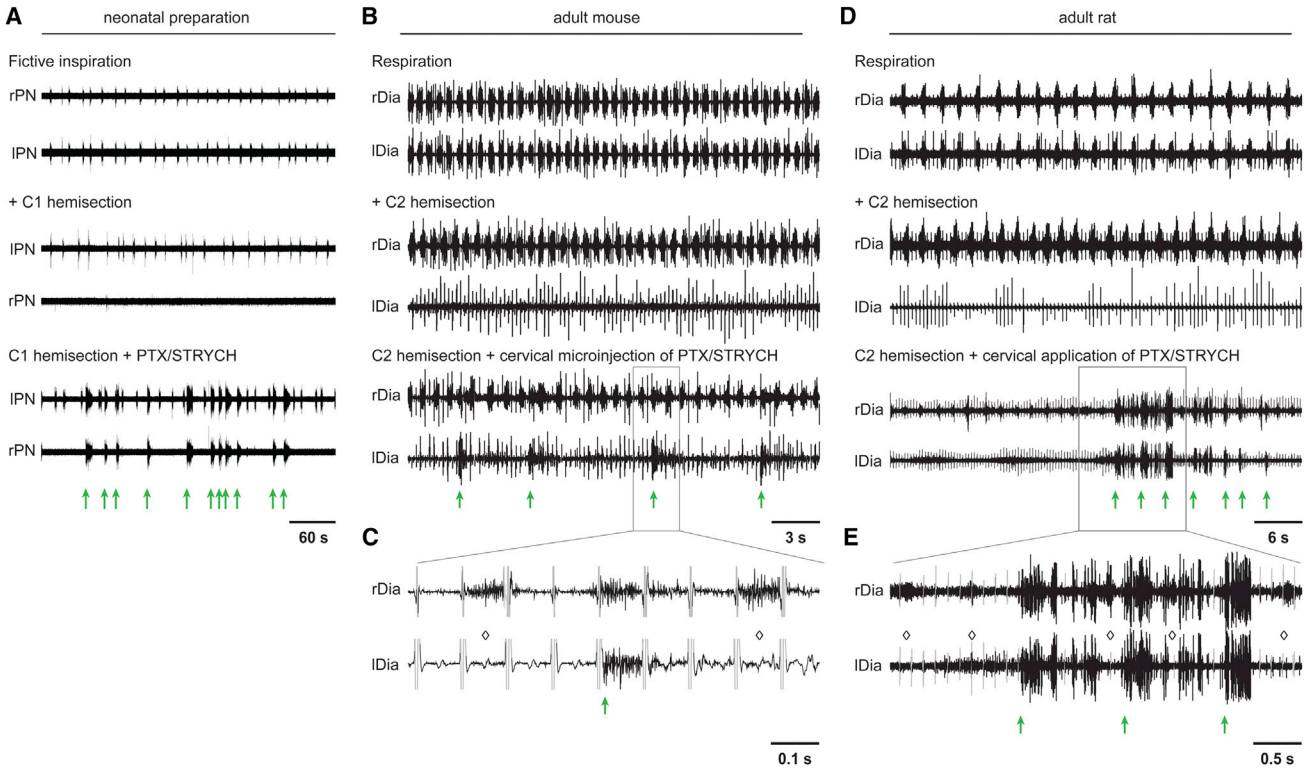

Figure 6. Spinal-Cord-Derived PMN Bursting Can Be Evoked after Adult Spinal Cord Injury

(A) In the ex vivo preparation from neonatal mice, left C1 hemisection eliminates fictive inspiration on the side ipsilateral to lesion, and application of PTX/STRYCH initiates spinal-cord-derived burst activity from the dennervated phrenic motor pool (green arrows distinguish spinal-cord-derived bursts from bursts of medullary origin). PTX/STRYCH-evoked bursting is, thus, dissociable from fictive inspiration (see also Figure 4A).

(B) In the adult mouse, left C2 hemisection eliminates left diaphragm activity (EKG artifact is still visible). Cervical microinjection (C3–C5, 3 sites; see Experimental Procedures) of PTX/STRYCH restores some PMN bursting in the paralyzed hemidiaphragm (n = 3). Green arrows indicate spinal-cord-derived PMN bursts.

(C) Inset from (B), with the EKG artifact highlighted in gray. Black portion of trace represents electromyogram (EMG). Diamonds indicate medullary derived respiratory bursts that fail to initiate PMN bursting on the side ipsilateral to the lesion.

(D) In the adult rat, left C2 hemisection eliminates left diaphragm activity (EKG artifact is still visible). Intrathecal injection of PTX/STRYCH at the cervical level restored some PMN bursting in the paralyzed hemidiaphragm in 3 of 4 rats.

(E) Inset from (D), with the EKG artifact highlighted in gray. Diamonds indicate medullary derived respiratory bursts that fail to initiate PMN bursting on the side ipsilateral to the lesion. In several instances, long spinal-cord-derived bursts were clearly spaced in between medullary derived inspiratory bursts.

DISCUSSION

Our data put to rest a lingering controversy—which has endured in the literature for more than a century—as to whether a "spinal respiratory rhythm generator" can initiate rhythmic inspiratory activity independent of supraspinal input (Brown-Séquard, 1860; Porter, 1895). Our data provide evidence against this hypothesis by demonstrating that, while PMN bursts of spinal cord origin can occur, they (1) are not spontaneous and can only be evoked under certain pharmacological conditions, (2) are not rhythmic (Figure 1F), (3) are anatomically and pharmacologically distinguishable from bona fide inspiratory circuits under the control of the preBötC, and (4) are likely derived from more caudal regions of the spinal cord associated with circuits of the locomotor CPG. The idea that a lack of inhibition could cause spontaneous PMN bursting is, perhaps, not surprising given that this occurs in premotor circuits of the lumbar cord, for which propriospinal circuits act as the basis for locomotion and effects of disinhibition are well described (Bracci et al., 1996). Nevertheless, these data are surprising in the context of a vast literature on PMNs, which are thought to derive their dominant excitatory input from supraspinal neurons of the rVRG. Our data, thus, lead to several exciting new hypotheses concerning the physiological role(s) for episodic spinal-cord-derived PMN bursts.

One possibility is that a caudally derived excitatory burst module is specifically associated with PMN control under certain circumstances. This could be related to premotor circuits anatomically positioned caudal to C8, such as those associated with control of sympathetic preganglionic neurons or intercostal motor neurons. Alternatively, an excitatory circuit that coordinates bilaterally symmetric motor neuron activity throughout the rostrocaudal extent of the spinal cord—but is dissociable from rhythmic respiratory circuits of the brainstem—might represent a substrate for innate behavioral responses such as startle. In point, hyperekplexia is an exaggerated startle disorder in humans associated with dysfunction of glycinergic transmission

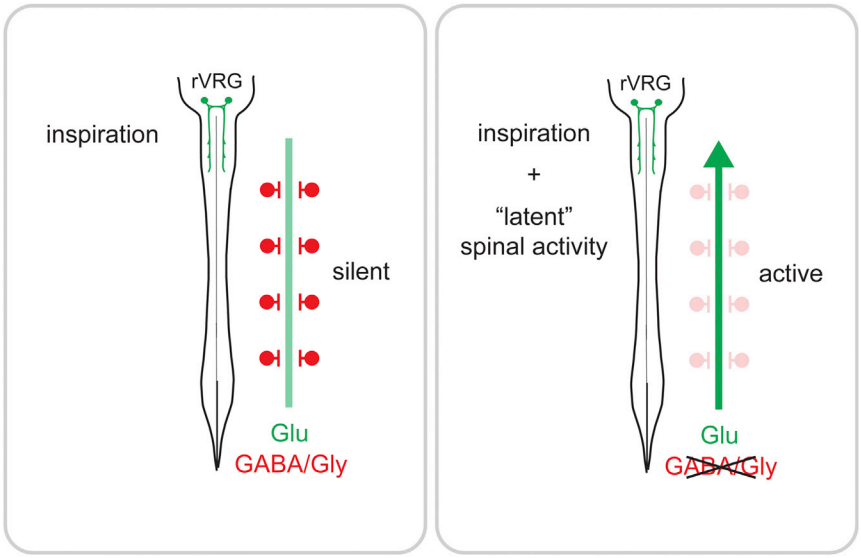

Figure 7. Summary of Findings
Two independent premotor networks control PMN activity post-natally: a descending, bulbospinal inspiratory network under control of the preBötC and a second "latent" network that exhibits spontaneous activity after suppression of GABA/glycinergic synaptic transmission.

(Rees et al., 2006). In contrast to these hypothetical roles, there is strong evidence that such spinal-cord-derived PMN burst activity does occur in situations of increased network excitability. Two well-described cases of increased network excitability exist physiologically: first, during embryogenesis, spinal circuits are highly excitable due to depolarizing action of GABA/glycine (Jean-Xavier et al., 2007). Second, SCI results in a variety of membrane and/or synaptic changes as well as anatomical remodeling that causes increased network excitability (Bellardita et al., 2017; Buttry and Goshgarian, 2014).

Low-frequency, long-duration bursts propagate within the spinal cord during embryogenesis as early as embryonic day (E)12 (Hanson and Landmesser, 2003; Momose-Sato et al., 2012a, 2012b; Myers et al., 2005). Interestingly, PMNs exhibit activity-dependent intramuscular nerve branching and innervation of the diaphragm during this early stage of embryogenesis (E12.5–E13.5; Brandon et al., 2003). Here, evoked acetylcholine (ACh) release from PMNs (rather than spontaneous vesicle fusion) regulates diaphragm innervation (Usiak and Landmesser, 1999; Washbourne et al., 2002). This evoked release is likely caused by spinal waves of propagating burst activity since activation of PMNs by the preBötC occurs much later at E15–E15.5 (Thoby-Brisson et al., 2009). Although waves of propagating burst activity during embryogenesis exhibit a number of similarities to those we observe in the disinhibited spinal cord, a notable difference is that burst activity during embryogenesis is generated chiefly by excitatory cholinergic rather than glutamatergic synaptic transmission (Hanson and Landmesser, 2003; Momose-Sato et al., 2012a, 2012b). The mechanisms underlying transition from acetylcholine to glutamate as the primary excitatory neurotransmitter in the spinal cord are not understood; however, evidence that glutamatergic networks compensate for loss of acetylcholine transmission in *ChAT*$^{-/-}$ embryos, and that proper assembly of locomotor networks is disrupted in *ChAT*$^{-/-}$ embryos, suggests that downregulation of cholinergic signaling may help to instruct the development of future glutamatergic premotor networks (Myers et al., 2005).

These data lend support to the hypothesis that the diffuse excitatory spinal circuit that can generate PMN activity post-natally might represent a "latent" or "holdover" network from development.

Increased excitation after SCI can lead to adverse outcomes, including muscle spasticity and/or autonomic dysreflexia (Bellardita et al., 2017; Ueno et al., 2016). An emergent view is that spasticity is caused by recruitment of disparate populations of excitatory neurons into functional circuits—leading to enhanced excitation independent of motor neuron excitability or inhibition (Bellardita et al., 2017). Interestingly, cervical SCI in human C4 tetraplegic patients is sometimes accompanied by diaphragm spasticity (Silver and Lehr, 1981). Moreover, we have observed occasional diaphragm spasticity after SCI in the adult rat in the context of experimental manipulations aimed at restoring function to the chronically denervated phrenic motor pool (P.M. Warren and J.S., unpublished data). It has been difficult to understand why diaphragm spasticity occurs, since premotor networks controlling phrenic bursting have been thought to reside in the medulla. These medullary networks should be relatively insensitive to lesion of the cervical spinal cord, suggesting a different origin of spastic activity. Recent transynaptic tracing experiments initiated in PMNs after C2 hemisection injury have demonstrated extensive anatomical plasticity in PMN premotor networks (Buttry and Goshgarian, 2014). The origin of diaphragm spasticity after adult SCI could, thus, be due to heightened engagement of a pre-existing spinal network that directs PMN bursting independently of descending bulbospinal input.

Excitingly, the same mechanisms that cause network dysfunction and/or spasticity might also be harnessed toward restoration of normal circuit function. In recent years, restoring diaphragm function after SCI has become a model system for understanding functional regeneration beyond the glial scar (Alilain et al., 2011; Cregg et al., 2014), because normal function of PMNs is controlled by direct monosynaptic connection with neurons of the rVRG (Davies et al., 1985; Duffin and van Alphen, 1995; Ellenberger and Feldman, 1988; Ellenberger et al., 1990). This model presents a somewhat simpler system (versus locomotion or micturition) for understanding how regenerating axons engage circuits caudal to a spinal cord lesion. In two examples from our previous work, we observed recovery of diaphragm function after hemiparalysis, which seemed to involve the contribution of interneuronal networks (Alilain et al., 2008, 2011). These results were perplexing at the time, because we did not understand that a spinal cord network could evoke PMN bursting

independently of bona fide inspiration, as our present study has shown (Alilain et al., 2008, 2011). Thus, those attempting to enhance regeneration of axons toward restoration of a "simple" motor behavior may need to consider the dynamic interplay between intact networks and networks that undergo dramatic reorganization caudal to a spinal lesion.

Finally, future experiments aiming to identify spinal PMN excitatory burst populations in more anatomical detail could lead to a diaphragm "pacing" device (Huang et al., 2016; Kowalski et al., 2013). We demonstrate pacing of spinal-cord-derived PMN bursting at a rate similar to that of fictive inspiration; given considerable technical advancements, this proof of concept could be therapeutically relevant in vivo after cervical SCI. Toward identification of PMN excitatory burst populations, our finding that spontaneous PMN burst activity is eliminated upon transection at C8 may be useful. In point, Kowalski and colleagues recently demonstrated that PMN unit activity—as opposed to burst activity demonstrated here—could be evoked by epidural stimulation at spinal cord level T2 (Kowalski et al., 2013). Altogether, our data provide new insight into PMN premotor network organization and establish a conceptual framework for targeting treatment and recovery of diaphragm function after cervical SCI.

EXPERIMENTAL PROCEDURES

For a full description of all methods, see the Supplemental Experimental Procedures.

Animals

All animal procedures were performed in accordance with Case Western Reserve University or University of Kentucky College of Medicine Institutional Animal Care and Use Committee (IACUC) guidelines. Mice were obtained from Jackson Laboratory. *Vglut2*^{Cre} or *ChAT*^{Cre} mice were crossed to *R26R*$^{ChR2\text{-}EYFP}$, *R26R*^{EYFP}, or *Tau*$^{lsl\text{-}LacZ}$ mice. Ex vivo experiments were carried out in P2–P4 male and female mice. Experiments in adult mice were performed in >8-week-old male and female mice. Sprague-Dawley rats were obtained from Charles River Laboratories. Rat experiments were performed in adult females >8 weeks old.

Ex Vivo Electrophysiology

After cryoanesthesia, rapid dissection was carried out in oxygenated Ringers solution. The hindbrain and spinal cord were exposed by ventral laminectomy, and the phrenic nerves were dissected free. Suction electrodes were attached to phrenic nerves and/or ventral roots from L2. A Polychrome V monochromator (Till Photonics) was used for photostimulation. The light intensity used in this study was ~0.20 mW/mm^2. We used the following drugs: NMDA (7 μM), 5HT (8 μM), PTX (10 μM), STRYCH (0.3 μM), CNQX (20 μM), AP5 (20 μM), DAMGO (2 μM), riluzole (10 μM), and d-tubocurarine (10 μM).

Histology

Retrograde tracing of PMNs was performed as described previously (Mantilla et al., 2009). Spinal cord tissue was fixed in 4% paraformaldehyde for 30 min and sectioned in the transverse plane at 20 μm. We used primary antibodies against GFP or ChAT. For X-gal staining, sections were incubated overnight at 37°C in X-gal staining buffer. In situ hybridization was performed as described previously (Philippidou et al., 2012). A *Vglut2* probe was generated from a cDNA library with the following primers: 5′-tggagaagaagcaggacaac and 5′-TAATACGACTCACTATAGGGgccagaacatgtaccagacc.

C2 Hemisection and Diaphragm Electromyogram

After anesthesia, bipolar recording electrodes were inserted into the left and right hemidiaphragms to record baseline diaphragm activity. C2 hemisection was performed just caudal to the C2 dorsal root. In mice, 250 nL of PTX (50 mM)/STRYCH (30 mM) was injected at 3 sites in levels C3–C5 on the side ipsilateral to the lesion at a depth of 1 mm. In rats, we injected 10 μL PTX/STRYCH intrathecally at the level of the C2 hemisection.

Analysis and Statistics

Representative raw traces are presented. Phase diagrams were constructed as previously described (Kjaerulff and Kiehn, 1996). Details on statistical tests used for each experiment can be found can be found in the accompanying figure legend. n represents the number of biological replicates (animals) for each group, unless stated otherwise.

SUPPLEMENTAL INFORMATION

Supplemental Information includes Supplemental Experimental Procedures and five figures and can be found with this article online at https://doi.org/10.1016/j.celrep.2017.09.076.

AUTHOR CONTRIBUTIONS

Conceptualization, J.M.C., L.T.L., and J.S.; Methodology, J.M.C., W.J.A., and P.P.; Investigation, J.M.C., K.A.C., L.E.H., R.S.J.M., D.R.S., and M.E.; Writing – Original Draft, J.M.C.; Writing – Review & Editing, J.M.C., L.T.L., and J.S.; Supervision – W.J.A., P.P., L.T.L., and J.S.; Funding Acquisition, J.M.C., W.J.A., P.P., L.T.L., and J.S.

ACKNOWLEDGMENTS

This work was supported by NSF grant DGE-0951783 (to J.M.C.), start-up from the University of Kentucky College of Medicine (to W.J.A.), NIH grant NS101105 (to W.J.A.), start-up from Case Western Reserve University (to P.P.), the Mt. Sinai Foundation (to P.P.), NIH grant NS085037 (to P.P.), NIH grant NS074199 (to L.T.L.), and NIH grant NS025713 (to J.S.). We thank Jing Qiang You for technical assistance and Thomas (TED) Dick, Philippa Warren, and Christopher Wilson for helpful commentary and discussion.

Received: May 4, 2017
Revised: August 8, 2017
Accepted: September 24, 2017
Published: October 17, 2017

REFERENCES

Alilain, W.J., Li, X., Horn, K.P., Dhingra, R., Dick, T.E., Herlitze, S., and Silver, J. (2008). Light-induced rescue of breathing after spinal cord injury. J. Neurosci. *28*, 11862–11870.

Alilain, W.J., Horn, K.P., Hu, H., Dick, T.E., and Silver, J. (2011). Functional regeneration of respiratory pathways after spinal cord injury. Nature *475*, 196–200.

Barber, R.P., Phelps, P.E., Houser, C.R., Crawford, G.D., Salvaterra, P.M., and Vaughn, J.E. (1984). The morphology and distribution of neurons containing choline acetyltransferase in the adult rat spinal cord: an immunocytochemical study. J. Comp. Neurol. *229*, 329–346.

Bellardita, C., Caggiano, V., Leiras, R., Caldeira, V., Fuchs, A., Bouvier, J., Löw, P., and Kiehn, O. (2017). Spatiotemporal correlation of spinal network dynamics underlying spasms in chronic spinalized mice. eLife *6*, e23011.

Bracci, E., Ballerini, L., and Nistri, A. (1996). Localization of rhythmogenic networks responsible for spontaneous bursts induced by strychnine and bicuculline in the rat isolated spinal cord. J. Neurosci. *16*, 7063–7076.

Brandon, E.P., Lin, W., D'Amour, K.A., Pizzo, D.P., Dominguez, B., Sugiura, Y., Thode, S., Ko, C.P., Thal, L.J., Gage, F.H., and Lee, K.F. (2003). Aberrant patterning of neuromuscular synapses in choline acetyltransferase-deficient mice. J. Neurosci. *23*, 539–549.

Brown-Séquard, C.E. (1860). Course of Lectures on the Physiology and Pathology of the Central Nervous System: Delivered at the Royal College of Surgeons of England in May, 1858 (Collins).

Buttry, J.L., and Goshgarian, H.G. (2014). Injection of WGA-Alexa 488 into the ipsilateral hemidiaphragm of acutely and chronically C2 hemisected rats reveals activity-dependent synaptic plasticity in the respiratory motor pathways. Exp. Neurol. *261*, 440–450.

Coglianese, C.J., Peiss, C.N., and Wurster, R.D. (1977). Rhythmic phrenic nerve activity and respiratory activity in spinal dogs. Respir. Physiol. *29*, 247–254.

Cregg, J.M., DePaul, M.A., Filous, A.R., Lang, B.T., Tran, A., and Silver, J. (2014). Functional regeneration beyond the glial scar. Exp. Neurol. *253*, 197–207.

Davies, J.G., Kirkwood, P.A., and Sears, T.A. (1985). The detection of monosynaptic connexions from inspiratory bulbospinal neurones to inspiratory motoneurones in the cat. J. Physiol. *368*, 33–62.

Decima, E.E., von Euler, C., and Thoden, U. (1969). Intercostal-to-phrenic reflexes in the spinal cat. Acta Physiol. Scand. *75*, 568–579.

Dobbins, E.G., and Feldman, J.L. (1994). Brainstem network controlling descending drive to phrenic motoneurons in rat. J. Comp. Neurol. *347*, 64–86.

Duffin, J., and van Alphen, J. (1995). Bilateral connections from ventral group inspiratory neurons to phrenic motoneurons in the rat determined by cross-correlation. Brain Res. *694*, 55–60.

Ellenberger, H.H., and Feldman, J.L. (1988). Monosynaptic transmission of respiratory drive to phrenic motoneurons from brainstem bulbospinal neurons in rats. J. Comp. Neurol. *269*, 47–57.

Ellenberger, H.H., Feldman, J.L., and Goshgarian, H.G. (1990). Ventral respiratory group projections to phrenic motoneurons: electron microscopic evidence for monosynaptic connections. J. Comp. Neurol. *302*, 707–714.

Ghali, M.G.Z., and Marchenko, V. (2016). Patterns of phrenic nerve discharge after complete high cervical spinal cord injury in the decerebrate rat. J. Neurotrauma *33*, 1115–1127.

Gray, P.A., Rekling, J.C., Bocchiaro, C.M., and Feldman, J.L. (1999). Modulation of respiratory frequency by peptidergic input to rhythmogenic neurons in the preBötzinger complex. Science *286*, 1566–1568.

Hägglund, M., Borgius, L., Dougherty, K.J., and Kiehn, O. (2010). Activation of groups of excitatory neurons in the mammalian spinal cord or hindbrain evokes locomotion. Nat. Neurosci. *13*, 246–252.

Hanson, M.G., and Landmesser, L.T. (2003). Characterization of the circuits that generate spontaneous episodes of activity in the early embryonic mouse spinal cord. J. Neurosci. *23*, 587–600.

Huang, R., Baca, S.M., Worrell, J.W., Liu, X., Seo, Y., Leiter, J.C., and Lu, D.C. (2016). Modulation of respiratory output by cervical epidural stimulation in the anesthetized mouse. J. Appl. Physiol. *121*, 1272–1281.

Jean-Xavier, C., Mentis, G.Z., O'Donovan, M.J., Cattaert, D., and Vinay, L. (2007). Dual personality of GABA/glycine-mediated depolarizations in immature spinal cord. Proc. Natl. Acad. Sci. USA *104*, 11477–11482.

Kjaerulff, O., and Kiehn, O. (1996). Distribution of networks generating and coordinating locomotor activity in the neonatal rat spinal cord in vitro: a lesion study. J. Neurosci. *16*, 5777–5794.

Kowalski, K.E., Hsieh, Y.H., Dick, T.E., and DiMarco, A.F. (2013). Diaphragm activation via high frequency spinal cord stimulation in a rodent model of spinal cord injury. Exp. Neurol. *247*, 689–693.

Lane, M.A., White, T.E., Coutts, M.A., Jones, A.L., Sandhu, M.S., Bloom, D.C., Bolser, D.C., Yates, B.J., Fuller, D.D., and Reier, P.J. (2008). Cervical prephrenic interneurons in the normal and lesioned spinal cord of the adult rat. J. Comp. Neurol. *511*, 692–709.

Lipski, J. (1984). Is there electrical coupling between phrenic motoneurons in cats? Neurosci. Lett. *46*, 229–234.

Lipski, J., Duffin, J., Kruszewska, B., and Zhang, X. (1993). Upper cervical inspiratory neurons in the rat: an electrophysiological and morphological study. Exp. Brain Res. *95*, 477–487.

Lois, J.H., Rice, C.D., and Yates, B.J. (2009). Neural circuits controlling diaphragm function in the cat revealed by transneuronal tracing. J. Appl. Physiol. *106*, 138–152.

Mantilla, C.B., Zhan, W.Z., and Sieck, G.C. (2009). Retrograde labeling of phrenic motoneurons by intrapleural injection. J. Neurosci. Methods *182*, 244–249.

Mentis, G.Z., Alvarez, F.J., Bonnot, A., Richards, D.S., Gonzalez-Forero, D., Zerda, R., and O'Donovan, M.J. (2005). Noncholinergic excitatory actions of motoneurons in the neonatal mammalian spinal cord. Proc. Natl. Acad. Sci. USA *102*, 7344–7349.

Momose-Sato, Y., Nakamori, T., and Sato, K. (2012a). Spontaneous depolarization wave in the mouse embryo: origin and large-scale propagation over the CNS identified with voltage-sensitive dye imaging. Eur. J. Neurosci. *35*, 1230–1241.

Momose-Sato, Y., Nakamori, T., and Sato, K. (2012b). Pharmacological mechanisms underlying switching from the large-scale depolarization wave to segregated activity in the mouse central nervous system. Eur. J. Neurosci. *35*, 1242–1252.

Myers, C.P., Lewcock, J.W., Hanson, M.G., Gosgnach, S., Aimone, J.B., Gage, F.H., Lee, K.F., Landmesser, L.T., and Pfaff, S.L. (2005). Cholinergic input is required during embryonic development to mediate proper assembly of spinal locomotor circuits. Neuron *46*, 37–49.

Nishimaru, H., Restrepo, C.E., Ryge, J., Yanagawa, Y., and Kiehn, O. (2005). Mammalian motor neurons corelease glutamate and acetylcholine at central synapses. Proc. Natl. Acad. Sci. USA *102*, 5245–5249.

Peña, F., Parkis, M.A., Tryba, A.K., and Ramirez, J.M. (2004). Differential contribution of pacemaker properties to the generation of respiratory rhythms during normoxia and hypoxia. Neuron *43*, 105–117.

Philippidou, P., Walsh, C.M., Aubin, J., Jeannotte, L., and Dasen, J.S. (2012). Sustained Hox5 gene activity is required for respiratory motor neuron development. Nat. Neurosci. *15*, 1636–1644.

Porter, W.T. (1895). The path of the respiratory impulse from the bulb to the phrenic nuclei. J. Physiol. *17*, 455–485.

Rees, M.I., Harvey, K., Pearce, B.R., Chung, S.K., Duguid, I.C., Thomas, P., Beatty, S., Graham, G.E., Armstrong, L., Shiang, R., et al. (2006). Mutations in the gene encoding GlyT2 (SLC6A5) define a presynaptic component of human startle disease. Nat. Genet. *38*, 801–806.

Reinoso, M.A., Sieck, G.C., and Hubmayr, R.D. (1996). Respiratory muscle coordination in acute spinal dogs. Respir. Physiol. *104*, 29–37.

Silver, J.R., and Lehr, R.P. (1981). Dyspnoea during generalised spasms in tetraplegic patients. J. Neurol. Neurosurg. Psychiatry *44*, 842–845.

Smith, J.C., Ellenberger, H.H., Ballanyi, K., Richter, D.W., and Feldman, J.L. (1991). Pre-Bötzinger complex: a brainstem region that may generate respiratory rhythm in mammals. Science *254*, 726–729.

Talpalar, A.E., Endo, T., Löw, P., Borgius, L., Hägglund, M., Dougherty, K.J., Ryge, J., Hnasko, T.S., and Kiehn, O. (2011). Identification of minimal neuronal networks involved in flexor-extensor alternation in the mammalian spinal cord. Neuron *71*, 1071–1084.

Thoby-Brisson, M., Karlén, M., Wu, N., Charnay, P., Champagnat, J., and Fortin, G. (2009). Genetic identification of an embryonic parafacial oscillator coupling to the preBötzinger complex. Nat. Neurosci. *12*, 1028–1035.

Tresch, M.C., and Kiehn, O. (2000). Motor coordination without action potentials in the mammalian spinal cord. Nat. Neurosci. *3*, 593–599.

Ueno, M., Ueno-Nakamura, Y., Niehaus, J., Popovich, P.G., and Yoshida, Y. (2016). Silencing spinal interneurons inhibits immune suppressive autonomic reflexes caused by spinal cord injury. Nat. Neurosci. *19*, 784–787.

Usiak, M.F., and Landmesser, L.T. (1999). Neuromuscular activity blockade induced by muscimol and d-tubocurarine differentially affects

the survival of embryonic chick motoneurons. J. Neurosci. *19*, 7925–7939.

Viala, D., Vidal, C., and Freton, E. (1979). Coordinated rhythmic bursting in respiratory and locomotor muscle nerves in the spinal rabbit. Neurosci. Lett. *11*, 155–159.

Washbourne, P., Thompson, P.M., Carta, M., Costa, E.T., Mathews, J.R., Lopez-Benditó, G., Molnár, Z., Becher, M.W., Valenzuela, C.F., Partridge, L.D., and Wilson, M.C. (2002). Genetic ablation of the t-SNARE SNAP-25 distinguishes mechanisms of neuroexocytosis. Nat. Neurosci. *5*, 19–26.

Zimmer, M.B., and Goshgarian, H.G. (2007). GABA, not glycine, mediates inhibition of latent respiratory motor pathways after spinal cord injury. Exp. Neurol. *203*, 493–501.

Cell Reports, Volume *21*

Supplemental Information

A Latent Propriospinal Network Can Restore Diaphragm Function after High Cervical Spinal Cord Injury

Jared M. Cregg, Kevin A. Chu, Lydia E. Hager, Rachel S.J. Maggard, Daimen R. Stoltz, Michaela Edmond, Warren J. Alilain, Polyxeni Philippidou, Lynn T. Landmesser, and Jerry Silver

Supplemental Figures

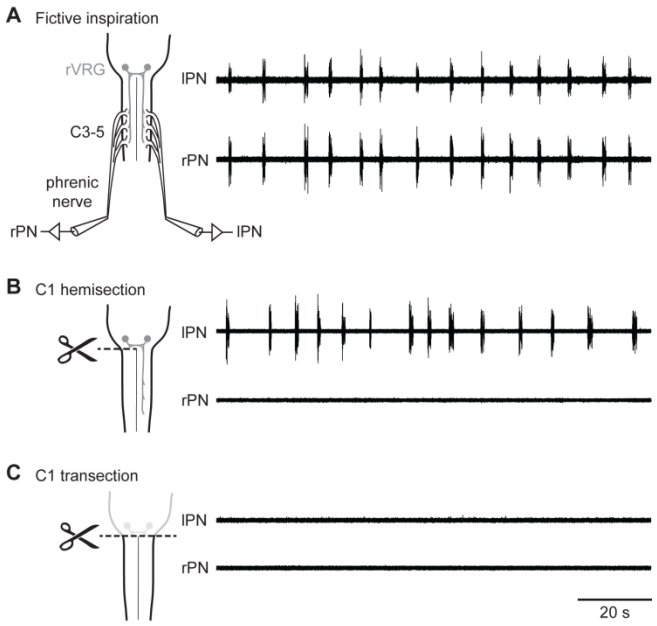

Figure S1. An *ex vivo* model of spinal cord injury recapitulates hallmark features of the adult descending respiratory system. Related to Figure 1.

(A) In the *ex vivo* spinomedullary preparation, fictive inspiratory activity is observed from right and left phrenic nerves (n = 8), note synchronous left/right bursting. Inspiratory rate is depressed relative to *in vivo* conditions due to lack of vagal feedback as well a recording temperature of 23-26^{o}C.

(B) Right C1 hemisection eliminates fictive inspiration only on the side ipsilateral to the lesion (rPN, n = 8).

(C) Complete C1 transection eliminates fictive inspiratory activity in both phrenic nerves (n = 8).

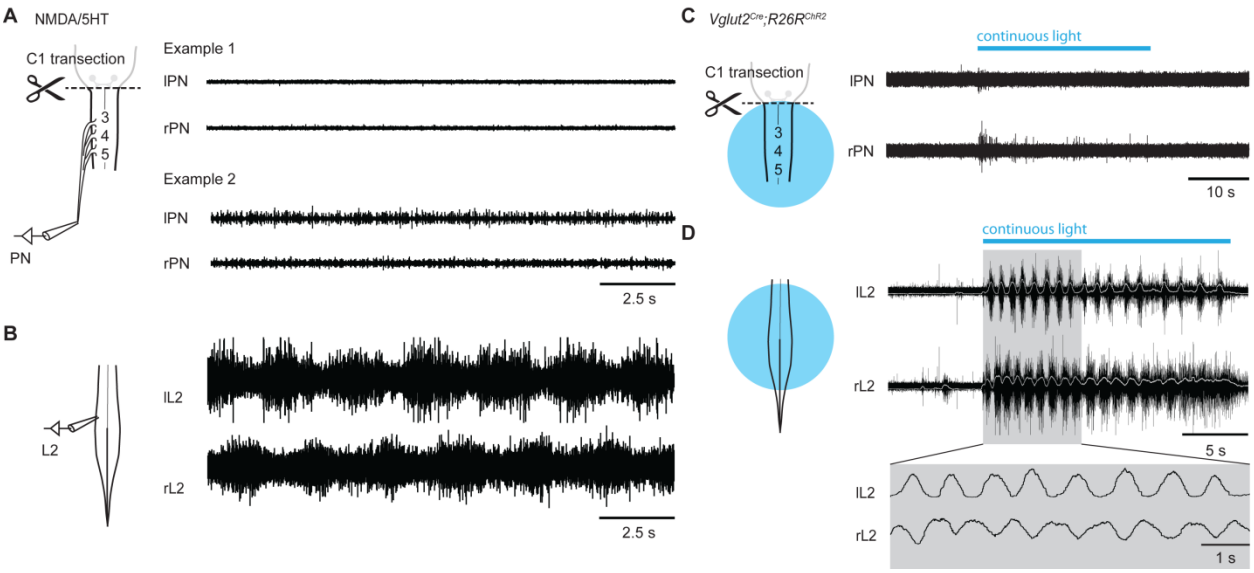

Figure S2. Increased excitation using pharmacology or optogenetics results in modest unit activity from PMNs. Related to Figure 1.

(A) After C1 transection, bath application of NMDA/5HT resulted in PMN unit activity in 50% of cases (Example 2, *n* = 2/4). We did not observe any PMN burst activity in response to application of NMDA/5HT.

(B) In contrast, bath application of NMDA/5HT resulted in robust locomotor-like burst activity from lumbar roots (bottom); i.e. left/right alternation of bursts is observed.

(C) After C1 transection, photostimulation of cervical Vglut2+ interneurons evoked modest unit activity from PMNs (top; best example). No PMN burst activity was observed in response to stimulation of cervical Vglut2+ neurons.

(D) In contrast, photostimulation of lumbar Vglut2+ neurons immediately evoked fictive locomotor activity in L2 ventral roots (bottom). Left/right alternation of burst pattern is visible.

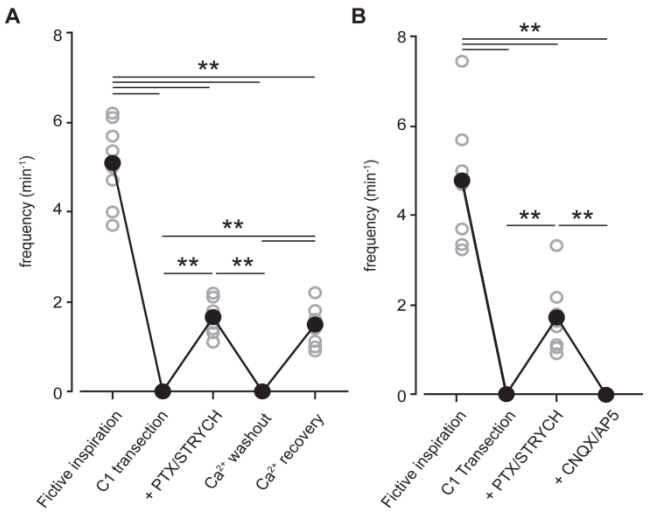

Figure S3. Spinal cord PMN bursting requires excitatory presynaptic input. Related to Figure 2.

(A) Ca^{2+} washout abolishes spontaneous spinal cord derived PMN bursting evoked by blockade of fast inhibitory neurotransmission. n = 8 mice, U = 64 for each significant comparison where $^{**}P < 0.01$, Mann-Whitney U test with Bonferroni correction for multiple comparisons.

(B) Bath application of antagonists of NMDA (AP5) and non-NMDA (CNQX) glutamate receptors abolishes spontaneous spinal cord derived PMN bursting. n = 8 mice, $^{**}P < 0.01$, U = 62.5 for inspiration vs. PTX/STRYCH and U = 64 for every other significant comparison, Mann-Whitney U test with Bonferroni correction.

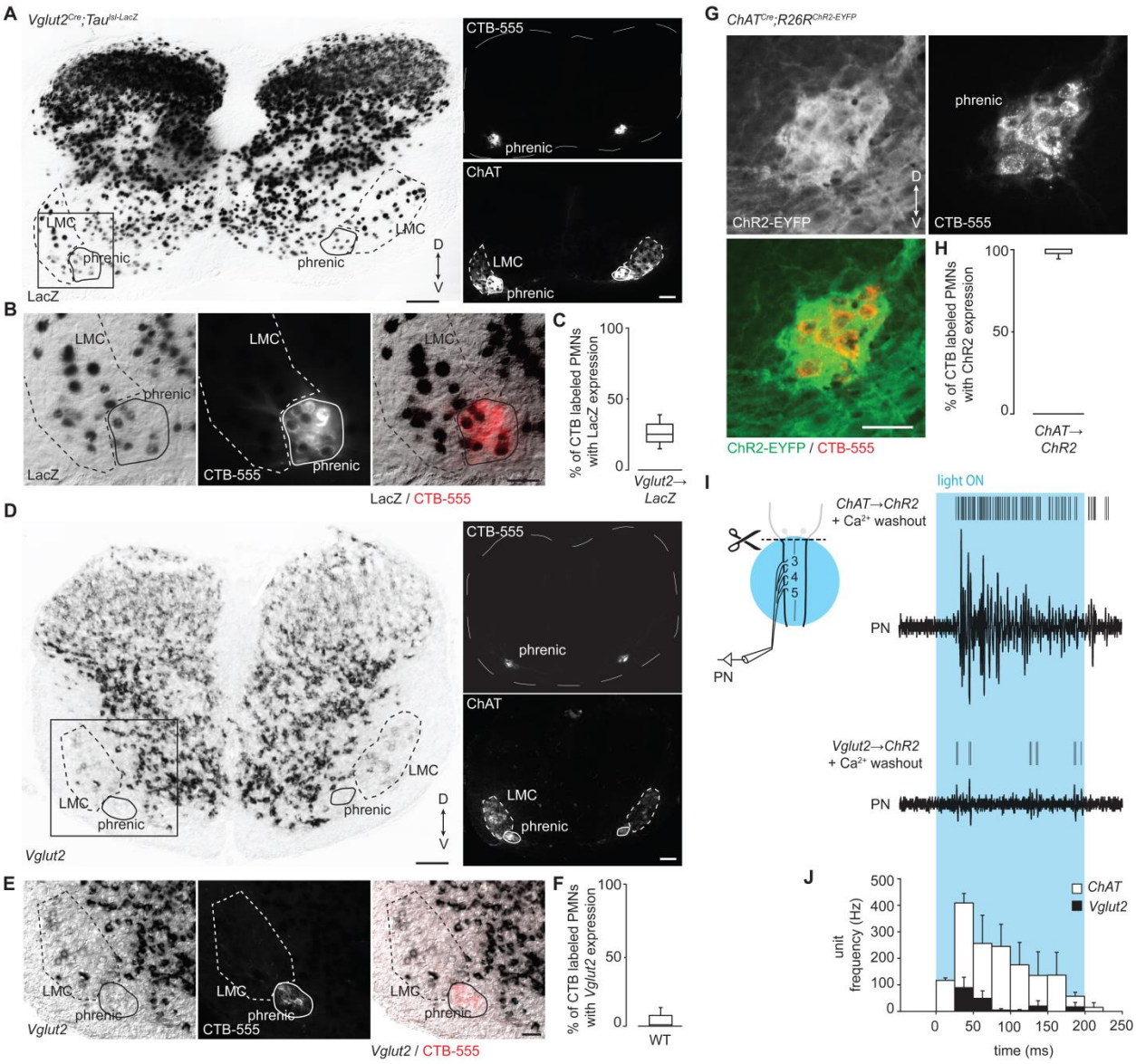

Figure S4. *Vglut2*^{Cre}- and *ChAT*^{Cre}-mediated recombination in PMNs. Related to Figures 2 and 3.

(A) Characterization of *Vglut2*^{Cre} allele. *Vglut2*^{Cre}-mediated recombination of a *Tau*$^{lsl\text{-}LacZ}$ reporter allele leads to LacZ expression in Cre-positive neurons. The phrenic motor nucleus and lateral motor column (LMC) were defined based on backlabeling of PMNs with CTB-555 (right, top) and by ChAT immunochemistry (right, bottom). LacZ expression was observed in excitatory interneurons, as well as a subset of LMC motor neurons and PMNs. Scale bars = 100 µm.

(B) Inset from (A). A subset of CTB-labeled PMNs exhibited expression of LacZ. Scale bar = 50 µm.

(C) Percentage of CTB-labeled PMNs with LacZ expression. 50/184 neurons (27.2%), *n* = 4.

(D) *In situ* hybridization for *Vglut2* mRNA (left). The phrenic motor nucleus and lateral motor column (LMC) were defined based on CTB-555 labeling of PMNs (right, top) and ChAT immunochemistry (right, bottom) in an adjacent section. LMC motor neurons exhibited some expression of *Vglut2* mRNA whereas PMNs did not (representative

image based on n = 4 animals). Excitatory interneurons exhibited much higher expression of *Vglut2* than motor neurons. Scale bars = 100 µm.

(E) Inset from (D). CTB-labeled PMNs in the same section probed for *Vglut2*. Scale bar = 50 µm.

(F) Percentage of CTB-labeled PMNs with *Vglut2* expression. 4/104 neurons (3.8%), n = 4.

(G) In $ChAT^{Cre};R26R^{ChR2\text{-}EYFP}$ mice, retrogradely labeled PMNs (CTB-555, red) exhibited expression of ChR2-EYFP (green, visualized by staining for GFP). Scale bar = 50 µm.

(H) Percentage of CTB-labeled PMNs in $ChAT^{Cre};R26R^{ChR2\text{-}EYFP}$ mice with ChR2-EYFP expression. 216/218 neurons (99.1%), n = 7.

(I) PMN unit activity evoked by photostimulation of $ChAT^{Cre};R26R^{ChR2}$ vs. $Vglut2^{Cre};R26R^{ChR2}$ PMNs. In the absence of Ca^{2+}, photostimulation of ChAT→ChR2 PMNs evoked robust unit activity (bars at top show units detected in the raw trace below). In contrast, photostimulation of Vglut2→ChR2 PMNs evoked only modest PMN unit activity.

(J) Quantification of PMN units evoked by photostimulation of ChAT→ChR2 vs. Vglut2→ChR2 PMNs. n = 3 for $ChAT^{Cre};R26R^{ChR2}$ preparations, and n = 4 for $Vglut2^{Cre};R26R^{ChR2}$ preparations.

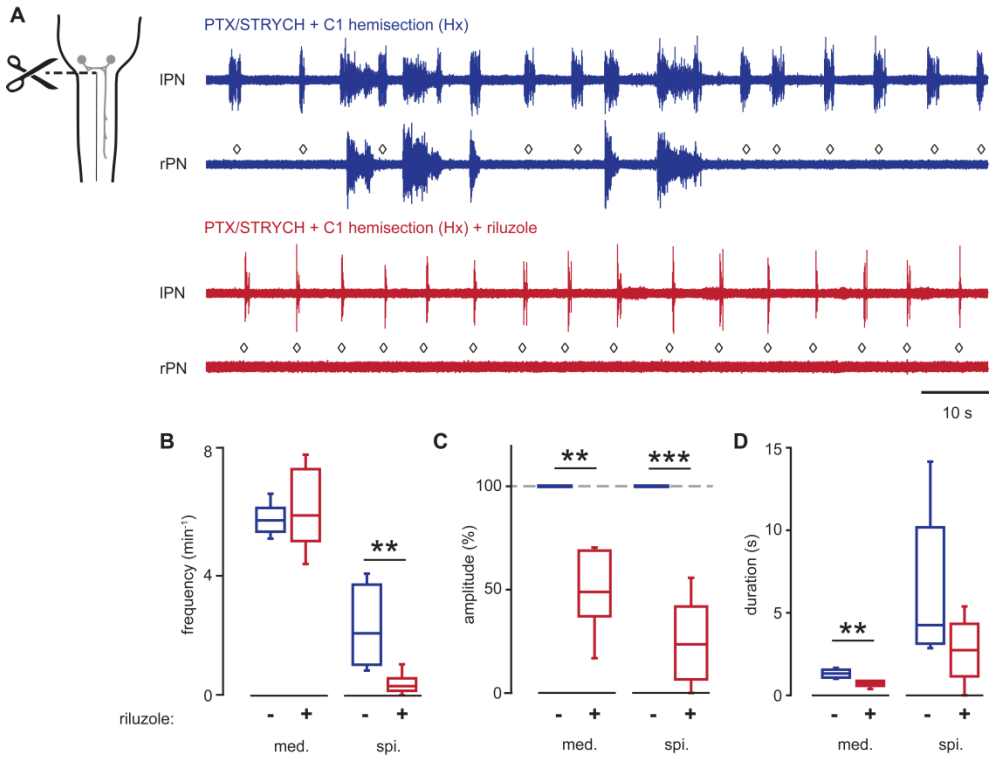

Figure S5. Spinal cord derived bursts are dependent on persistent sodium current (I_{NaP}). Related to Figure 4.

(A) A right C1 hemisection (blue traces) eliminated medullary derived bursts from the right phrenic nerve (◊, bottom trace). The remaining right PMN bursts were synchronous with the longer duration bursts on the intact side, and thus represent spinal cord derived bursts. Riluzole addition (10 µM, blocks I_{NaP} nonselectively, red traces) largely blocked spinal cord derived PMN bursts from both sides (rPN/lPN) without affecting the frequency of medullary derived bursts (lPN). ◊ indicates absence of medullary derived PMN burst on the side ipsilateral (rPN) to C1 hemisection.

(B) Selective depression of spinal cord (spi.) derived burst frequency in the presence of riluzole (n = 8; P = 0.4073 and t_{14} = 0.9 for med., two-tailed t-test; **P = 0.0022 and U = 61.5 for spi., Mann-Whitney U test).

(C) Riluzole application reduced the amplitude of medullary (n = 8, **P = 0.0084 and U = 56, Mann-Whitney U test) derived bursts but to a lesser extent than the spinal cord derived bursts (n = 8, ***P = 0.00041 and U = 64, Mann-Whitney U test).

(D) Riluzole application reduced the duration of medullary derived bursts (med.; n = 8; **P = 0.0038 and t_{14} = 3.5 for med., two-tailed t-test; P = 0.0829 and U = 49 for spi., Mann-Whitney U test).

Supplemental Experimental Procedures

Contact for Reagent and Resource Sharing

Further information and requests for resources should be directed to and will be fulfilled by the Lead Contact, Jerry Silver (jxs10@case.edu).

Experimental Models

All animal procedures were performed in accordance with Case Western Reserve University or University of Kentucky College of Medicine Institutional Animal Care and Use Committee (IACUC) guidelines.

Vglut2^{Cre} (Jackson Laboratories, stock #016963, STOCK Slc17a6$^{tm2(cre)Lowl}$/J), *ChAT*^{Cre} (#006410, B6;129S6-Chat$^{tm2(cre)Lowl}$/J), *R26R*$^{ChR2\text{-}EYFP}$ (#012569, B6;129S-Gt(ROSA)26Sor$^{tm32(CAG\text{-}COP4*H134R/EYFP)Hze}$/J), *R26R*^{EYFP} (#007903, B6.Cg-Gt(ROSA)26Sor$^{tm3(CAG\text{-}EYFP)Hze}$/J), and *Tau*$^{lsl\text{-}LacZ}$ (#021162, B6.129P2-Mapt^{tm2Arbr}/J) mice were obtained from Jackson Laboratories and maintained on a mixed background. Genotyping was conducted according to Jax strain-specific genotyping protocols. *Vglut2*^{Cre} or *ChAT*^{Cre} mice were crossed to homozygous *R26R*$^{ChR2\text{-}EYFP}$ reporter mice to direct ChR2-EYFP expression to glutamatergic or cholinergic neurons, respectively. Given dense labeling of neuropil due to strong axonal trafficking of ChR2-EYFP in *Vglut2*^{Cre}*;R26R*$^{ChR2\text{-}EYFP}$ mice (data not shown), we used homozygous *R26R*^{EYFP} or *Tau*$^{lsl\text{-}LacZ}$ reporter mice to label glutamatergic neuronal soma with EYFP or LacZ, respectively. Animals heterozygous for Cre recombinase and heterozygous for ChR2-EYFP, EYFP, or LacZ alleles were used for these experiments. We carried out experiments that did not require genetic perturbations in wild type C57BL/6J mice (#000664). Animals were assigned to groups based on genotype. Experiments and analysis were performed with prior knowledge of genotype. *Ex vivo* experiments were carried out in P2-4 male/female mice. Experiments in adult mice were performed in >8 week old male/female mice.

Sprague-Dawley rats were purchased from Charles River Laboratories, Inc. Rat experiments were performed in adult females >8 weeks old.

Dissection

P2-4 mice were cryoanesthetized and rapid dissection was carried out in 23-26 °C oxygenated Ringers solution. Solution was composed of 128 mM NaCl, 4 mM KCl, 21 mM $NaHCO_3$, 0.5 mM NaH_2PO_4, 2 mM $CaCl_2$, 1 mM $MgCl_2$, and 30 mM D-glucose and was equilibrated by bubbling in 95% O_2/5% CO_2. The hindbrain and spinal cord were exposed by ventral laminectomy, and phrenic nerves exposed and dissected free of connective tissue. Phrenic nerves were identified as the only medially projecting nerves arising from the brachial plexus. A transection at the pontomedullary boundary rostral to the anterior inferior cerebellar artery was used to initiate fictive inspiration. C1 transection/hemisection were performed at the level of the C1 ventral root, which is caudal to the obex.

***Ex vivo* Electrophysiology and Photostimulation**

Recording experiments were performed under continuous perfusion of oxygenated Ringers solution (14 ml min^{-1}, 23-26 °C). Suction electrodes were attached to phrenic nerves (rPN/lPN) and/or ventral roots from lumbar segment 2 (L2). Signal was band-pass filtered from 30 Hz to 1 kHz using Grass amplifiers, amplified 10,000-fold, and sampled at a rate of 50 kHz with a Digidata 1440A (Molecular Devices). A Polychrome V monochromator (Till Photonics) was used for photostimulation, where blue light (wavelength 473 nm, 10 nm bandwidth) was directed at the spinal cord using a fiberoptic light guide (Till Photonics). The spatial extent of light illumination and scatter in the transverse plane is represented in experimental schematics (Figures 2A, 3C, 5D, S2C, and S2D). Light intensity was measured with a photodiode (Cat# S120C, Thorlabs) coupled to a power meter (Cat# PM100D, Thorlabs). The light intensity used in this study was ~0.20 mW mm^{-2}.

Drugs

NMDA (7 µM, Sigma), 5-hydroxytryptophan (5HT, 8 µM, Sigma), picrotoxin (PTX, 10 µM, Sigma, $GABA_AR$ antagonist), strychnine hydrochloride (STRYCH, 0.3 µM, Sigma, GlyR antagonist), CNQX (20 µM, Sigma, non-NMDA glutamatergic receptor antagonist), AP5 (20 µM, Sigma, NMDAR antagonist), D-Ala^2-*N*-Me-Phe^4-glycol^5-enkephalin (DAMGO, 2 µM, Sigma, µ-opioid receptor agonist), riluzole (10 µM, Tocris), and d-Tubocurarine (10 µM, Tocris, AChR antagonist).

Retrograde Tracing

Retrograde tracing of PMNs was performed as described previously (Mantilla et al., 2009), but adapted to neonatal mice. P0 mice were cryoanesthetized, and a 33 gauge Hamilton syringe was used to deliver 10 µl of CTB-555 into the pleural space (ThermoFisher Cat# C34776, 2 mg/ml). Pups were allowed to recover on a heating pad before returning to their home cage.

Immunochemistry and X-gal Staining

Spinal cord tissue from P4 mice was dissected free and fixed in 4% paraformaldehyde for 30 min. 20 µm thick transverse spinal cord sections were obtained using a cryostat. Sections were blocked for 2 h in 5% normal goat or donkey serum and 0.1% triton-X100, and subsequently incubated overnight with rabbit anti-GFP (ThermoFisher Cat# 11122, 1:500) and/or goat anti-ChAT (Chemicon Cat# AB144P) primary antibodies. After 3-4 washes in 1x PBS + 0.1% triton-X100, tissue was incubated overnight with appropriate Alexa fluor secondary antibodies from ThermoFisher or Jackson ImmunoResearch. After 3-4 more washes, coverslips were mounted using CITIFLOUR Af1 medium. For X-gal staining, spinal cord sections were washed in PBS and subsequently incubated overnight at 37^{o}C in X-gal staining buffer as follows: 1x PBS, 1:5000 IGEPAL CA-630, 5 mM potassium ferrocyanide (Sigma Aldrich, Cat# P9387), 5 mM potassium ferricyanide (Sigma Aldrich, Cat# P8131), 0.01 wt/v % sodium dodecyl sulfate (SDS), and 2.5 mM 5-bromo-4-chloro-3-indolyl β-D-galactopyranoside (X-gal, Sigma-Aldrich, B4252). X-gal stained sections were washed in PBS, and slides were then mounted with coverslips. Imaging was performed on a Leica upright fluorescence/brightfield scope.

***In Situ* Hybridization**

In situ hybridization was performed as described (Philippidou et al., 2012). P4 spinal cord was dissected free and fixed for 2 h in 4% paraformaldehyde. 20 µm thick transverse spinal cord sections were obtained using a cryostat. To generate an *in situ* probe for *Vglut2*, RNA was collected from P2 mouse spinal cord (Thermo Fisher Scientific Cat# AM1931), and reverse transcribed to cDNA (Applied Biosystems Cat# 4368814). A 710 bp template for *in vitro* transcription was amplified using platinum *Taq* polymerase with the following primers: 5'-tggagaagaagcaggacaac and 5'-TAATACGACTCACTATAGGGgccagaacatgtaccagacc, where the underlined sequence is the T7 promoter. A PCR cleanup was performed, and a DIG-labeled *Vglut2* probe was generated by *in vitro* transcription (Sigma-Aldrich Cat# 11175025910) followed by column purification (Sigma-Aldrich Cat# GE27-5330-01). Tissue sections were hybridized with the *Vglut2* probe, and subsequently incubated with an alkaline phosphatase labeled antibody against DIG (Sigma-Aldrich Cat# 11093274910). Color was developed using a NBT/BCIP solution (Sigma-Aldrich Cat# 11681451001).

C2 Hemisection and Diaphragm EMG

Mice were anesthetized with a ketamine (80 mg/kg) and xylazine (10 mg/kg) cocktail administered intraperitoneally. Rats were anesthetized with urethane (1.2 g/kg) administered intraperitoneally in doses of 0.8 g/kg and 0.4 g/kg separated by 1 h. A laparotomy was performed to expose the diaphragm. Bipolar recording electrodes were inserted into the left and right hemidiaphragm to record baseline inspiratory activity. Signal was amplified using Grass amplifiers, and acquired in Spike2 using a CED1401 acquisition system (Cambridge Electronic Design, Ltd.). After baseline recording, a multilevel dorsal laminectomy was performed over the C2-5 spinal cord. The dura and arachnoid mater were opened, and a C2 hemisection was performed with angled microscissors just caudal to the C2 dorsal root. We established the completeness of the C2 hemisection lesion by diaphragm EMG recording. In mice, we used a Nanoject (Drummond Scientific) to deliver 250 nl of PTX (50 mM)/STRYCH (30 mM) at 3 sites in levels C3-5 on the side ipsilateral to the lesion. Injections were performed at a depth of 1 mm. In rats, we injected 10 ul PTX (50 mM)/STRYCH (30 mM) intrathecally at the level of the C2 hemisection.

Analysis

Data was recorded using pCLAMP 10 software (Molecular Devices) and analyzed in Spike2 (Cambridge Electronic Design, Ltd.). Signal was processed to remove DC drift. Poincaré plots in Figure 1 were used to examine variability in burst cycle. Using group data from 8 animals, we calculated IBI_n, IBI_{n+1} matrix values using a custom Perl script (available upon request), and plotted contours in Origin 8 (OriginLab Corporation). Raster plot in Figure 2 was constructed in R (R Project), where trials are aligned by light onset, and the timing and duration of individual bursts are represented by black rectangles (using the rect() function in R). Gray boxes were used to highlight independent biological replicates. Burst probability was calculated continuously (averaged every 0.1 s over 24 trials, bin = 5 s) using a custom Perl script (available upon request). Phrenic motor neuron positioning in Figure 3 was quantified relative to the central canal (0,0) for both right and left phrenic motor pools. We combined right/left data by vertical transformation, calculated contour matrix values using a custom Perl script (available upon request), and plotted

contours in Origin 8 (OriginLab Corporation). Burst amplitude in Figures 4 and S5 was quantified in rectified and integrated (time constant = 0.2 s) traces before/after drug application, and without movement of the recording electrode between conditions. To account for variability in recording signal between preparations, amplitude is presented as a percentage of pre-drug baseline (100%). Phase diagrams in Figure 5 were constructed as previously described (Kjaerulff and Kiehn, 1996), where 0 represents in-phase (synchronous) and π represents out of phase (asynchronous) bursting. In Figure 6, EKG artifact was reduced using ECGDelete script from Cambridge Electronic Design, Ltd.

Statistics

Statistical analysis was performed in JMP version 11 (SAS). Minimum sample size needed to obtain statistical significance was determined by power analysis, and experiments were performed with at least this minimum number of animals. A Shapiro-Wilk test was used to determine whether data sets exhibited a normal Gaussian distribution. For data not abiding to a normal distribution (sometimes due to boundary constraints), a Mann-Whitney U test was used for pairwise comparisons. For data exhibiting a normal distribution, a Brown-Forsythe test was used to determine whether groups exhibited equivalent variance. In cases of equivalent variance, a two-tailed t-test was used for comparisons between 2 groups, and a one-way ANOVA test was performed for >2 groups. A Tukey-Kramer HSD test was used *post hoc* to compare individual pairs and assign levels of significance. If variances were unequal, Welch's ANOVA test was performed to account for unequal standard deviations. Bonferroni correction was used for multiple comparisons in Mann-Whitney U and Welch ANOVA. $P < 0.05$ was considered to be statistically significant, where $*P < 0.05$, $**P < 0.01$, $***P < 0.001$. Descriptive data is presented as mean ± standard error mean. Box and whisker plots were used to visualize data, where whiskers represent range excluding outliers. *n* represents the number of biological replicates (animals) for each group, unless stated otherwise. Details on statistical tests used for each experiment can be found can be found in the accompanying figure legend.